2006-06

Hermite-Gaussian modes and mirror distortions in the free electron laser

Vigil, Ricardo.

Monterey California. Naval Postgraduate School

NAVAL POSTGRADUATE SCHOOL
Monterey, California

THESIS

HERMITE-GAUSSIAN MODES AND MIRROR DISTORTIONS IN THE FREE ELECTRON LASER

by

Ricardo Vigil

June 2006

Thesis Advisor: William Colson
Co-Advisor: Robert Armstead

THIS PAGE INTENTIONALLY LEFT BLANK

REPORT DOCUMENTATION PAGE

Form Approved OMB No. 0704-0188

1. AGENCY USE ONLY (*Leave blank*)	2. REPORT DATE	3. REPORT TYPE AND DATES COVERED
	June 2006	Master's Thesis

4. TITLE AND SUBTITLE Hermite-Gaussian Modes and Mirror Distortions in the Free Electron Laser

5. FUNDING NUMBERS

6. AUTHORS Vigil, Ricardo

7. PERFORMING ORGANIZATION NAME(S) AND ADDRESS(ES)
Naval Postgraduate School
Monterey CA 93943-5000

8. PERFORMING ORGANIZATION REPORT NUMBER

9. SPONSORING/MONITORING AGENCY NAME(S) AND ADDRESS(ES)

10. SPONSORING/MONITORING AGENCY REPORT NUMBER

11. SUPPLEMENTARY NOTES The views expressed in this thesis are those of the author and do not reflect the official policy or position of the Department of Defense or the U.S. Government.

12a. DISTRIBUTION/AVAILABILITY STATEMENT
Approved for public release; distribution is unlimited.

12b. DISTRIBUTION CODE

13. ABSTRACT(*maximum 200 words*)

The free electron laser (FEL) is proposed to meet the Navy's need for a speed-of-light high energy laser weapon capable of engaging a variety of targets including anti-ship cruise missiles, small boats, and theater ballistic missiles. A key attribute of FELs is good optical beam quality; in other words, they operate in only a few of the lowest-order transverse Gaussian modes. For weapons applications, a good mode quality is desired because it delivers the highest intensity on target ensuring a high level of lethality. A few higher-order modes can arise from the interaction of the electron beam with the optical beam, or from misalignments of the electron beam or resonator mirrors. High intensity on FEL optics can lead to mirror distortion due to heating and insufficient cooling of the mirror substrate. Mirror distortions, including astigmatism, can cause higher-order modes to appear affecting FEL performance. Therefore, it is important to quantify these higher-order modes because doing so uniquely identifies the optical field and may allow for corrective optics to single out the best modes for FEL lethality. This thesis will review free electron laser theory, and for the first time develop analytical solutions to quantify Hermite-Gaussian higher-order modes, develop a diagnostic for modal analysis, and determine the tolerance limits on mirror distortions.

14. SUBJECT TERMS free electron laser, high energy laser, astigmatism hermite, gaussian, modes, higher order modes, hermite-gaussian

15. NUMBER OF PAGES 106

16. PRICE CODE

17. SECURITY CLASSIFICATION OF REPORT	18. SECURITY CLASSIFICATION OF THIS PAGE	19. SECURITY CLASSIFICATION OF ABSTRACT	20. LIMITATION OF ABSTRACT
Unclassified	Unclassified	Unclassified	UL

NSN 7540-01-280-5500

Standard Form 298 (Rev. 2-89)
Prescribed by ANSI Std. 239-18 298-102

THIS PAGE INTENTIONALLY LEFT BLANK

Approved for public release; distribution is unlimited

HERMITE-GAUSSIAN MODES AND MIRROR DISTORTIONS IN THE FREE ELECTRON LASER

Ricardo Vigil
Lieutenant Commander, United States Navy
B.S., Rensselaer Polytechnic Institute, 1996

Submitted in partial fulfillment of the
requirements for the degree of

MASTER OF SCIENCE IN PHYSICS

from the

NAVAL POSTGRADUATE SCHOOL
June 2006

Author: Ricardo Vigil

Approved by: William Colson
Thesis Advisor

Robert Armstead
Co-Advisor

James Luscombe
Chairman, Department of Physics

THIS PAGE INTENTIONALLY LEFT BLANK

ABSTRACT

The free electron laser (FEL) is proposed to meet the Navy's need for a speed-of-light high energy laser weapon capable of engaging a variety of targets including anti-ship cruise missiles, small boats, and theater ballistic missiles. A key attribute of FELs is good optical beam quality; in other words, they operate in only a few of the lowest-order transverse Gaussian modes. For weapons applications, a good mode quality is desired because it delivers the highest intensity on target ensuring a high level of lethality. A few higher-order modes can arise from the interaction of the electron beam with the optical beam, or from misalignments of the electron beam or resonator mirrors. High intensity on FEL optics can lead to mirror distortion due to heating and insufficient cooling of the mirror substrate. Mirror distortions, including astigmatism, can cause higher-order modes to appear affecting FEL performance. Therefore, it is important to quantify these higher-order modes because doing so uniquely identifies the optical field and may allow for corrective optics to single out the best modes for FEL lethality.

This thesis will review free electron laser theory, and for the first time develop analytical solutions to quantify Hermite-Gaussian higher-order modes, develop a diagnostic for modal analysis, and determine the tolerance limits on mirror distortions.

THIS PAGE INTENTIONALLY LEFT BLANK

DISCLAIMER

This thesis was created using LaTeX 2_ε on an Apple PowerBook G4. For information LaTeX or the code developed for this thesis, please feel free to contact me at my permanent email address: vigilr@alum.rpi.edu.

THIS PAGE INTENTIONALLY LEFT BLANK

TABLE OF CONTENTS

LIST OF FIGURES

LIST OF TABLES

THIS PAGE INTENTIONALLY LEFT BLANK

ACKNOWLEDGMENTS

¡Besos y abrazos, Mamá y Papá!

I would like to thank Professor Blau, Professor Armstead, and Professor Crooker for their help in preparing this thesis. I would like to thank my cousin, Dr. Dan, for some enlightening mathematical discussions. Special thanks to Professor Colson for giving me this great opportunity.

I also would like to acknowledge the Sailors and Marines on-station and on-watch....

THIS PAGE INTENTIONALLY LEFT BLANK

I. MOTIVATION

Previous Naval Postgraduate School (NPS) classroom studies have shown that the PHALANX close-in weapon system, used onboard US Navy ships as a last tier self-defense weapon, typically destroys an enemy missile at a distance of a few hundred meters from the ship. At that distance, NPS classroom studies have also shown a large probability that debris will cause collateral damage to the ship. A key factor in determining debris field collateral damage is *time*. An anti-ship cruise missile (ASCM) typically has a velocity of 1200 m/s. If it is detected at a nominal horizontal distance[1] of 15 km, then the ship has approximately 13 seconds to track and engage the missile. The probability of collateral damage stems from the fact that it takes several PHALANX rounds to destroy the missile. So, Naval interest in high energy lasers is clear: by engaging a target with a speed-of-light high energy laser weapon, the distance and time-to-engage increases considerably and the probability of collateral damage to the ship is reduced.

In order to "kill" a missile, about one liter of missile material must be destroyed. This will cause sufficient structural damage resulting in missile breakup. The amount of energy required for material ablation is on the order of one megawatt over a surface area of 100 cm^2 for a few seconds. If an ASCM, like the one described above, is detected at 15 km and engaged by a high energy laser, it would be destroyed in roughly five seconds at a distance of 9 km from the ship reducing the probability of collateral damage considerably giving the ship a large safety margin in time and distance.

Several U.S. Navy laser programs are currently investigating the feasibility of employing high energy lasers on board ships. The free electron laser (FEL) possesses

[1]Horizontal distance as a function of height of eye is given by $D_E(\text{nautical miles}) = 1.169\sqrt{\text{Height of eye (ft)}}$

many attributes that are in-line with the the Navy's vision of an all-electric ship with no munitions:

- High average power
- Can be designed over a range of wavelengths (IR through X-rays)
- Good optical beam quality
- High operational reliability
- No hazardous chemicals required for lasing medium
- Virtually limitless magazine depth
- Capable of engaging a variety of targets including ASCMs, small boats, and theater ballistic missiles

A key attribute of FELs is good optical beam quality; in other words, they operate in only a few of the lowest-order Gaussian modes. A key attribute of FELs is good optical beam quality; in other words, they operate in only a few of the lowest-order transverse Gaussian modes. For weapons applications, a good mode quality is desired because it delivers the highest intensity on target ensuring a high level of lethality. A few higher-order modes can arise from the interaction of the electron beam with the optical beam, or from misalignments of the electron beam or resonator mirrors. High intensity on FEL optics can lead to mirror distortion due to heating and insufficient cooling of the mirror substrate. Mirror distortions, including astigmatism, can cause higher-order modes to appear affecting FEL performance. Therefore, it is important to quantify these higher-order modes because doing so uniquely identifies the optical field and may allow for corrective optics to single out the best modes for FEL lethality.

This thesis will review free electron laser theory, and for the first time develop analytical solutions to quantify Hermite-Gaussian higher-order modes, develop a diagnostic for modal analysis, and determine the tolerance limits on mirror distortions.

II. FREE ELECTRON LASER SYSTEM

The free electron laser (FEL) system consists of many different components each of which involves very interesting physics. Figure 1 shows a basic systems diagram of the operating FEL at the Thomas Jefferson National Accelerator Facility (JLab). Let us walk through the operation of JLab's FEL. A pulsed beam of electrons in a vacuum is produced using a photoinjector. The beam of electrons are accelerated to near the speed of light in the superconducting accelerator using radio-frequency (RF) energy. Highly relativistic electrons are then "wiggled" in the undulator producing laser light where it is amplified by extracting energy from the electron beam within the optical resonator. The electron beam's remaining energy is recycled by having them enter the superconducting accelerator out of phase with the RF fields. Finally, the electron beam is directed to a beam dump.

At the heart of the FEL system are relativistic "free" electrons, i.e., not bound to any atom or molecule. The electrons travel in a vacuum much like in a cathode ray tube. Conventional lasers operate at specific frequencies because electrons can make transitions only between discrete energy levels. The electrons of an FEL are forced to vibrate through a spatial periodic magnetic field. The frequency of vibration can be changed by adjusting the magnetic field or by changing the speed of the electrons which in turn changes the laser light frequency.

In 1970 Dr. John Madey of Stanford University proposed what he termed a "free electron laser" using highly relativistic electrons to produce radiation in a magnetic undulator. Six years later Madey succeeded in demonstrating gain with a free electron laser with a 24 MeV electron beam and 5 m long undulator [2].

As an illustrative example of an operating FEL, Table I shows the current parameters at JLab. At the time of this writing, JLab has the most powerful free electron laser in the world at 10 kW. The wavelength is in the infrared around 2 - 4 μm.

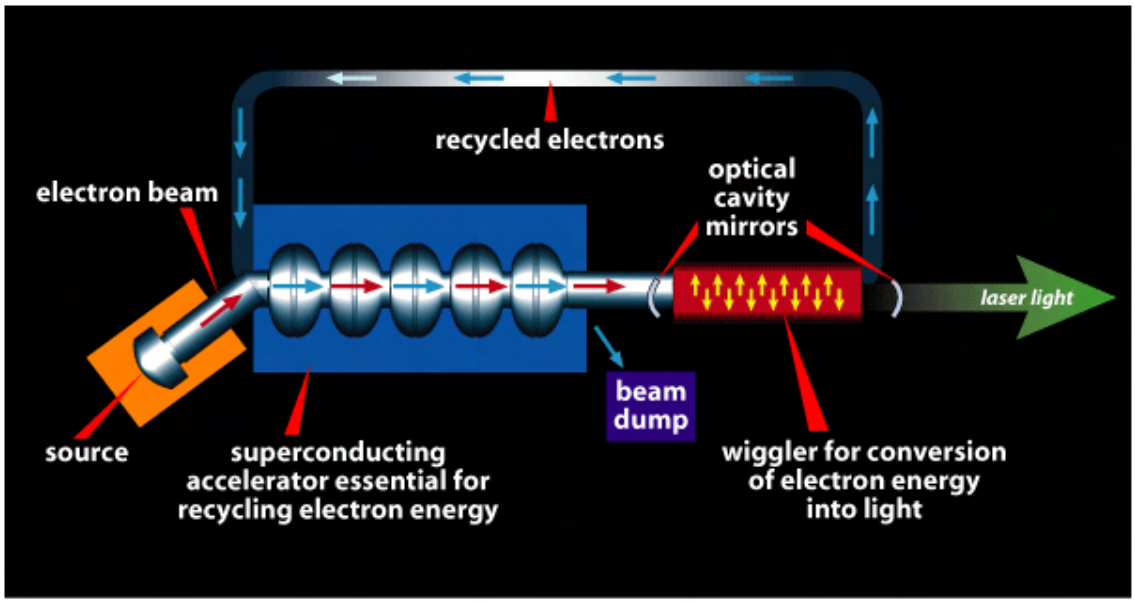

Figure 1. Free electron laser systems diagram highlighting major components from [1].

A. HOW DOES IT WORK?

For an FEL to work we need [4]:

- a beam of relativistic electrons,
- co-propagating in an optical field,
- through a series of spatially periodic magnets.

The undulator establishes electron oscillations that are transverse to its overall longitudinal motion. In a reference frame moving along the FEL axis with the electrons, it would appear that they are simply oscillating and radiating in all directions. In the laboratory frame the radiation is confined to a narrow forward cone whose angle is a function of the electron's speed, and is known as magnetic Bremsstrahlung radiation [2]. The radiation emitted is highly Doppler shifted due to the relativistic nature of the electrons and the wavelength is given by

$$\lambda = \lambda_o \frac{(K^2 + 1)}{2\gamma^2} \tag{II.1}$$

Optical Resonator	
Output power	10 kW
Length	32m
Wavelength	1.1μm
Waist radius	0.6 mm
Mode radius at mirror	1 cm
Quality factor	25 (4% outcoupling)
Rayleigh length	0.5 m
Max. intensity permissible on mirrors	200 kW/cm^2
Electron Beam	
Energy	111 MeV
Bunch charge	135 pC
Radius	0.2 mm
Peak current	340 A
Pulse length	0.12 mm
Undulator	
Period, λ_o	8 cm
Length	2.3
Number of periods	29
Undulator parameter, K	0.55

Table I. JLab FEL Parameters from [3].

where λ is the wavelength of the optical radiation, λ_o is the wavelength of the undulator magnetic field, γ is the Lorentz factor, K is a dimensionless parameter that is proportional to the undulator magnetic field strength. We will derive this equation in the next chapter.

The initial optical radiation given off by the oscillating electrons is known as spontaneous emission in the vernacular of conventional laser physics. The radiation from spontaneous emission is incoherent, meaning that, the wave packets emanating from each radiating electron are not in phase with adjacent wavepackets since each electron is randomly dispersed within the electron beam. Coherence evolves from this cacophony through mode competition with many passes through the undulator. The process of mode competition will be covered later.

At resonance, the electric field felt by the electrons oscillates at the same frequency and in the same plane as the electrons oscillating through the periodic undulator magnetic field. If the electric field and the electron's transverse motion is parallel, electrons will lose energy and slow down since work is being done *by* them. If the electric field and the electron's transverse motion is anti-parallel, electrons will gain energy and speed up since work is being done *on* them. The energy they lose or gain comes from the optical radiation field. The effect of electrons losing and gaining energy within each optical wavelength is a longitudinal bunching of electrons as some slow down and others speed up in each wavelength. The bunched electrons then emit radiation that is in phase and coherent. The intensity of the coherent radiation is much more powerful than the incoherent radiation [2].

Two key performance metrics of the FEL can now be introduced: extraction and gain. The fractional increase in optical radiation power in one pass of the undulator is defined as gain,

$$G = \frac{P - P_o}{P_o} \tag{II.2}$$

where the optical power, P, is measured at the end of the undulator and P_o is the power at the beginning of the undulator. As the FEL converts electron kinetic energy to optical radiation energy, the fractional energy extracted from the electron beam in one pass of the undulator is defined as extraction, η,

$$\eta = \frac{\text{Optical power}}{\text{Initial electron beam power}} \tag{II.3}$$

The optical gain must be sufficient to overcome loss and outcoupling. A larger extraction means the FEL requires less average current to achieve high power. Typical values for extraction and gain are 2% and 30%, respectively.

B. CONFIGURATIONS

When the undulator is bounded within two reflective mirrors, the configuration is known as an optical oscillator or resonator. The optical radiation field that

couples to the electron's motion can manifest itself through spontaneous emission. This radiation is collected within mirrors as shown in Figure 2. A partially reflective outcoupling mirror provides the optical feedback back into the undulator. Coherence develops through many passes of the optical field. The source of the optical radi-

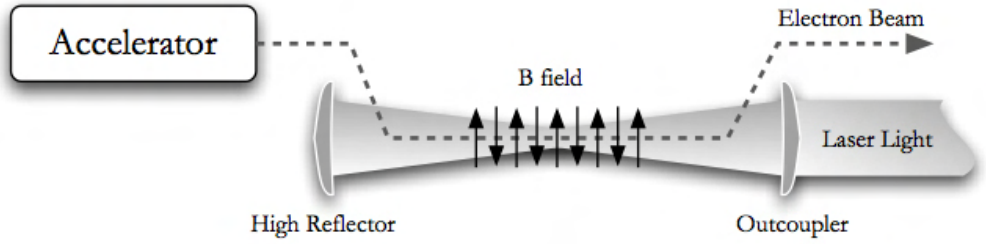

Figure 2. Free electron laser system in an oscillator configuration from [5].

ation field can also be an external laser in the case of an amplifier. An amplifier configuration makes use of a seed laser and typically a longer undulator. The longer undulator provides more gain and extraction in a single pass since only one pass is used. Coherence is established by the seed laser. Figure 3 shows a typical amplifier configuration.

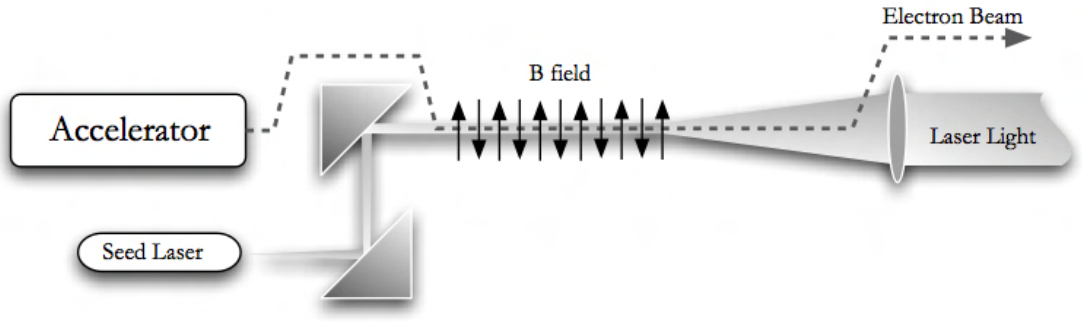

Figure 3. Free electron laser system in an amplifier configuration from [5].

C. COMPONENTS

1. Source

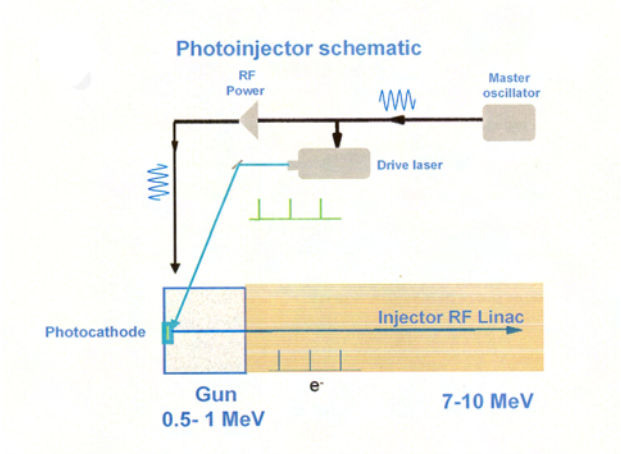

Figure 4. Schematic of a typical photoinjector from [6].

An FEL requires high peak current in order for coherent radiation to grow in amplitude. The source for free electrons is a photoinjector. A drive laser, usually a solid-state laser, is pulsed at a photocathode target. Through the photoelectric effect, electrons are literally blasted from the surface of a cathode and accelerated in an electric field to the linear accelerator. Since the drive laser fires at regular intervals (on the order of nanoseconds), electrons travel in pulses. Electrons at the terminus of the photoinjector have energies from 5 to 10 million electron-volts (MeV).

2. Accelerator

The linear accelerator (see Figure 5) has two functions: (1) accelerate electrons from the photoinjector to its final velocity (energy $\approx$ 100 MeV), and (2) recover energy from recycled electrons. The electrons are accelerated as they travel through the cavities in phase with the radio-frequency (RF) fields. At JLab, electron bundles from the photoinjector are accelerated using a superconducting RF linear accelerator to minimize waste heat. Energy is recovered from recycled electrons and given back to the RF field since they reenter the accelerator out of phase with the RF field.

Figure 5. JLab linear accelerator from [7]

3. Undulator

The undulator is a collection of spatially alternating permanent magnets that causes the electrons to wiggle transverse to their longitudinal motion. The transverse motion then couples to the optical electric field enabling work to be done on or by the optical radiation field. The magnets can be orientated linearly or helically as shown in Figure 6. Linear undulators produce linearly polarized light whose electric field oscillates in the same plane as the oscillating electrons. Helical undulators produce circularly polarized light whose electric field rotates along with the electrons enabling a coupling to occur.

4. Beam Dump

After energy is recovered from the recycled electrons in the linear accelerator, the electron beam is steered into a beam dump (see Figure 7). A beam dump is nothing more than a piece of notched metal that will absorb the remaining kinetic energy of the electron beam (on the order of several MeV). At at an average electron beam current of one ampere, about one megawatt must be absorbed. It is water-cooled on the non-vacuum side.

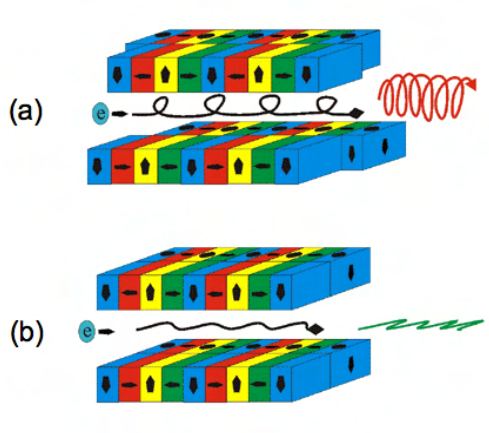

Figure 6. (a) Helical undulator resulting in circularly polarized light. (b) Linear undulator resulting in linearly polarized light from [8].

5. Optics

As mentioned in Table I, the maximum permissible intensity on the resonator mirrors is on the order of 200 kW/cm^2 to prevent mirror damage to the mirror's dielectric layers. In adequate or nonuniform mirror cooling may also warp the sapphire substrate thereby affecting FEL performance. FEL designs with a short Rayleigth length[1] have modes that expand so that the intensity on the mirrors is lessened. The entire optical system includes all the necessary beam directors to place laser energy on a target miles away from the ship.

[1]Rayleigh length is the distance the mode has to travel longitudinally from the waist so that the mode area doubles. Rayleigh length will be discussed in greater detail in Chapter IV.

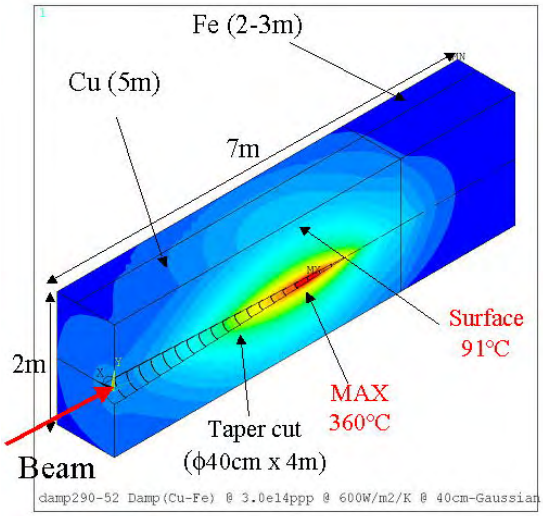

Figure 7. Beam dump from [9]

THIS PAGE INTENTIONALLY LEFT BLANK

III. FREE ELECTRON LASER THEORY

We will now develop in detail the mathematics that describes the operation of the free electron laser. In order to produce laser light we must cause electrons to oscillate through a Lorentz force interaction, bunch the electrons spatially for coherence, and finally, have sufficient electron-to-optical mode coupling for amplification and gain.

A. EQUATIONS OF MOTION

1. Relativistic Lorentz Force

In compact covariant notation, the relativistic Lorentz Force law[1] is

$$\frac{dp^\alpha}{dt'} = m\frac{dU^\alpha}{dt'} = -\frac{e}{c}F^{\alpha\beta}U_\beta \tag{III.1}$$

where $p^\alpha = (\gamma mc, \mathbf{p})$ is the four-momentum, $\gamma = 1/\sqrt{1 - v^2/c^2}$ is the Lorentz factor, $\mathbf{v}$ is the electron's velocity, m is the mass of the electron, $U_\beta = (\gamma c, -\gamma\mathbf{v})$ is the electron's four-velocity, $t' = t/\gamma$ is proper time, e is the magnitude of the electron's charge, c is the speed of light, and $F^{\alpha\beta}$ is the field-strength tensor with the components of the electric field, $\mathbf{E}$, and magnetic field, $\mathbf{B}$. Specifically,

$$F^{\alpha\beta} = \begin{pmatrix} 0 & -E_x & -E_y & -E_z \\ E_x & 0 & -B_z & B_y \\ E_y & B_z & 0 & -B_x \\ E_z & -B_y & B_x & 0 \end{pmatrix} \tag{III.2}$$

Let us describe the electron's trajectory in a helical undulator whose magnetic field along z is

$$\mathbf{B_u} = B_o(\cos k_o z, \sin k_o z, 0) \tag{III.3}$$

where B_o is the magnetic field amplitude, $k_o = 2\pi/\lambda_o$ is the undulator wavenumber, and λ_o is the undulator wavelength, i.e., the distance for one complete cycle of the

[1] [10], Chapter 11

undulator magnetic field. The corresponding electric and magnetic field of the optical radiation field is:

$$\mathbf{E_r} = E_o(\cos\psi, -\sin\psi, 0) \tag{III.4}$$

$$\mathbf{B_r} = E_o(\sin\psi, \cos\psi, 0) \tag{III.5}$$

where $\psi = kz - \omega t + \phi$, k is the optical wavenumber, $\omega = kc$ is the optical angular frequency, E_o is the field amplitude in cgs units, and ϕ is the optical phase.

If we combine Equations (III.3), (III.4), and (III.5), Equation (III.2) becomes

$$F^{\alpha\beta} = \begin{pmatrix} 0 & -E_o\cos\phi & E_o\sin\phi & 0 \\ E_o\cos\psi & 0 & 0 & B_o\sin k_o z + E_o\cos\phi \\ -E_o\sin\psi & 0 & 0 & -B_o\cos k_o z - E_o\sin\phi \\ 0 & -B_o\sin k_o z - E_o\sin\psi & B_o\cos k_o z + E_o\sin\psi & 0 \end{pmatrix} \tag{III.6}$$

Using Equations (III.1), (III.6), and

$$\boldsymbol{\beta} = \frac{\mathbf{v}}{c} \tag{III.7}$$

$$\gamma = \frac{1}{\sqrt{1-\beta^2}} \tag{III.8}$$

where $\boldsymbol{\beta}$ is dimensionless velocity and γ is the Lorentz factor. We can write down the spatial components of the force from Equation (III.1),

$$\begin{aligned} \frac{d(\gamma\boldsymbol{\beta}_\perp)}{dt} &= -\frac{e}{mc}[E_o(1-\beta_z)(\cos\psi, -\sin\psi, 0) + \beta_z B_o(-\sin k_o z, \cos k_o z, 0)] \\ \frac{d(\gamma\beta_z)}{dt} &= -\frac{e}{mc}[E_o(\beta_x\cos\psi - \beta_y\sin\psi) + B_o(\beta_x\sin k_o z - \beta_y\cos k_o z)] \end{aligned} \tag{III.9}$$

where we have made use of $\boldsymbol{\beta}_\perp = \beta_x\hat{\boldsymbol{\imath}} + \beta_y\hat{\boldsymbol{\jmath}}$. Since $\beta_z \approx 1$, $(1-\beta_z) \to 0$, we then drop the terms proportional to $E_o(1-\beta_z)$ compared to $\beta_z B_o$. Integrating the transverse equation gives (assuming perfect injection[2])

$$\boldsymbol{\beta}_\perp = \frac{-eB_o}{\gamma mc^2 k_o}(\cos k_o z, \sin k_o z, 0) = \frac{-eB_o\lambda_o}{2\pi\gamma mc^2}(\cos k_o z, \sin k_o z, 0) \tag{III.10}$$

[2]Perfection injection means that the electrons enter the undulator at precisely the correct angle such that its motion is exactly given by Equation (III.10) and constants of integration are zero.

We can clean this equation up a little if we identify the dimensionless undulator parameter, $K = eB_o\lambda_o/(2\pi mc^2)$ to write:

$$\boldsymbol{\beta}_\perp = \frac{-K}{\gamma}(\cos k_o z, \sin k_o z, 0) \tag{III.11}$$

We can now derive the energy exchange equation between the electrons and the optical field. With Equation (III.2), $dt' = dt/\gamma$ and $p^0 = \mathcal{E}/c = \gamma mc$, from relativistic kinematics[3], we can write down the zeroth component, or energy component, of Equation (III.1). For $\alpha = 0$, we have

$$\frac{dp^0}{d\tau} = -\frac{e}{c}F^{0\beta}U_\beta$$

so that

$$\gamma\frac{d}{dt}(\gamma mc) = -\frac{e}{c}(0, -\mathbf{E}) \cdot (\gamma c, -\gamma \mathbf{v})$$

and

$$\gamma\frac{d}{dt}(\gamma mc) = -\frac{e\gamma}{c}\mathbf{E} \cdot \mathbf{v}$$

giving

$$\frac{d\gamma}{dt} = -\frac{e}{mc}\boldsymbol{\beta} \cdot \mathbf{E} \tag{III.12}$$

Equation (III.12) describes how the the electron exchanges energy with the optical field. The electron's total energy, $\mathcal{E} = \gamma mc^2$, is a function of its rest mass and its speed (through γ). The undulator sets up electron motion in the transverse directions otherwise $\boldsymbol{\beta} \cdot \mathbf{E}$ would be zero.

Substituting Equations (III.4) and (III.11) into (III.12), we arrive at

$$\dot{\gamma} = \frac{eKE_o}{\gamma mc}\cos(k_o z + \psi) \tag{III.13}$$

[3] see [11], Chapter 1

Recall that $\psi = kz - \omega t + \phi$. If we define

$$\zeta \equiv (k_o + k)z - \omega t \tag{III.14}$$

as the electron phase, we have

$$\dot{\gamma} = \frac{eKE_o}{\gamma mc} \cos(\zeta + \phi) \tag{III.15}$$

We have arrived at an expression that describes energy exchange between the electron and optical field. Electron phase, ζ, is another way of describing the electron's position along the undulator axis with respect to the co-propagating optical wave. Notice that for $\cos(\zeta + \phi) > 0$, the electron energy increases (absorption); for values less than zero, the electron loses energy (stimulated emission).

2. Resonance Condition and Dimensionless Variables Introduced

Since the electron phase, ζ, is proportional to the electron position, z, let us define the dimensionless electron phase velocity as

$$\nu \equiv \dot{\zeta}\, L/c \tag{III.16}$$

where L is the length of the undulator. We can normalize the evolution of the electron's motion to the length of the undulator by defining a dimensionless time, $\tau = ct/L$. It is convenient when possible to normalize our equations on scales that are relevant to the physics being explored. For example, longitudinal length can be normalized to the length of undulator. Thus, τ takes on values from $0 \rightarrow 1$ from the beginning of the undulator to the end of the undulator. In the following sections, we will normalize transverse directions, optical field amplitude, and current density.

Returning to phase velocity, ν can also be expressed as

$$\nu = \overset{\circ}{\zeta} \tag{III.17}$$

where $(\overset{\circ}{.}) = d(\ldots)/d\tau$ is a derivative with respect to dimensionless time τ. Phase velocity, ν, is a measure of how fast the electron is moving longitudinally within an undulator period. We can now derive the resonance condition.

The resonance condition results in optimum energy exchange between the electron and the optical mode. This occurs when one wavelength of light passes over an electron as the electron travels through one undulator period. FEL resonance occurs when $\nu = 0$. Taking the time derivative of the electron phase gives us

$$\begin{aligned} \zeta &= (k_o + k)z - \omega t \\ \dot{\zeta} &= (k_o + k)\beta_z c - \omega \end{aligned} \tag{III.18}$$

Substituting this expression into the definition of electron phase velocity gives us

$$\nu = [(k_o + k)\beta_z c - \omega]\frac{L}{c} \tag{III.19}$$

For $\nu = 0$, we have

$$\begin{aligned} k &= \frac{k_o \beta_z}{(1 - \beta_z)} \\ \text{so that } \lambda &= \lambda_o \frac{(1 - \beta_z)}{\beta_z} \end{aligned} \tag{III.20}$$

where we have used $k = \omega/c$. So now let us find an expression for β_z in terms of physical parameters of the FEL. From Equation (III.11), $\beta_\perp = K/\gamma$, and the definition of the Lorentz factor, we have

$$\begin{aligned} \gamma &= \frac{1}{\sqrt{1 - \beta^2}} \\ \gamma^2 &= \frac{1}{1 - \beta_\perp^2 - \beta_z^2} \\ \gamma^2 &= \frac{1}{1 - \frac{K^2}{\gamma^2} - \beta_z^2} \end{aligned} \tag{III.21}$$

Solving for the electron velocity gives us

$$\beta_z = \sqrt{1 - \frac{1}{\gamma^2}(K^2 + 1)} \tag{III.22}$$

For highly relativistic electrons employed in an FEL, γ is typically ≈ 100, so we can make use of the binomial expansion[4] giving us

$$\begin{aligned} \beta_z &= \sqrt{1 - \frac{1}{\gamma^2}(K^2+1)} \\ \beta_z &\approx 1 - \frac{1}{2\gamma^2}(K^2+1) \end{aligned} \tag{III.23}$$

Returning to Equation (III.20), we then have,

$$\lambda = \lambda_o \frac{(K^2+1)}{2\gamma^2} \tag{III.24}$$

Here is an expression for the wavelength of the optical mode based on physical parameters that we can change (λ_o, K, γ): a clear example of the FEL's tunability. It is now understandable why the wavelength of the light is so much smaller (by a factor of $1/\gamma^2$) than the undulator period. This is physically plausible since the relativistic nature of the electrons causes them to see the undulator Lorentz-contracted by a factor of γ and Doppler-shifted light from the electrons' frame is then transformed to the lab frame reducing the wavelength by another factor of γ. Electrons see resonant forces from undulator and the optical field. The end result is the optical field is at a much higher frequency then the undulator's spatial frequency.

3. Pendulum Equation

We are now in a position to recast the equations in the previous sections into a form known as the pendulum equation. In this pendulum description, phase-space plotting becomes a natural and highly illustrative way of describing the electrons' motion and interaction with the optical mode. Starting with the phase velocity, we

[4]The binomial expansion for small x is given by

$$(1+x)^n = 1 + nx + \frac{n(n-1)}{2!}x^2 + \cdots$$

see [12] pp. 14 for more details

have

$$\nu = [(k_o + k)\beta_z - k]L = \overset{\circ}{\zeta} \tag{III.25}$$

$$\dot{\nu} = (k_o + k)\,\dot{\beta}_z\,L \tag{III.26}$$

So let us now calculate an expression for $\dot{\beta}_z$. From Equation (III.23),

$$\beta_z \approx 1 - \frac{1}{2\gamma^2}(K^2 + 1)$$

$$\dot{\beta}_z = -\frac{1}{2}(-2)\gamma^{-3}\frac{d\gamma}{dt}(K^2 + 1) \tag{III.27}$$

$$\dot{\beta}_z = \frac{\dot{\gamma}}{\gamma^3}(K^2 + 1) \tag{III.28}$$

But near resonance we have $(K^2 + 1)/\gamma^2 = 2\lambda/\lambda_o$, so Equation (III.28) becomes

$$\dot{\beta}_z = \frac{\dot{\gamma}}{\gamma}\frac{(K^2 + 1)}{\gamma^2}$$

$$\dot{\beta}_z = \frac{\dot{\gamma}}{\gamma}\frac{2\lambda}{\lambda_o} \tag{III.29}$$

Returning to Equation (III.26), substituting Equation (III.29), and using $k = 2\pi/\lambda$, we arrive at

$$\dot{\nu} = (k_o + k)\frac{\dot{\gamma}}{\gamma}\frac{2\lambda}{\lambda_o}L \tag{III.30}$$

$$\dot{\nu} = \frac{4\pi\lambda}{\lambda_o^2}\frac{\dot{\gamma}}{\gamma}L + \frac{4\pi}{\lambda_o}\frac{\dot{\gamma}}{\gamma}L \tag{III.31}$$

We can make the following substitutions and approximations: since the undulator period is much larger than the optical wavelength (i.e, $\lambda_o >> \lambda$), and since the first term is smaller than the second by a factor λ/λ_o, the first term is negligible. We define $|a| = 4\pi NeK|E|L/\gamma^2 mc^2$ as the dimensionless optical field amplitude, $L = N\lambda_o$, the length of the undulator, $dt = Ld\tau/c$, and substituting Equation (III.15), we finally arrive at

$$\overset{\circ}{\nu} = |a|\cos(\zeta + \phi) = \overset{\circ\circ}{\zeta} \tag{III.32}$$

The pendulum equation describes the motion of the electrons in phase space, (ζ, ν).

4. Phase Space

Phase space diagrams are used in many physical problems. For example, in a simple pendulum, the angular displacement, $\theta(t)$, and its angular velocity, $\nu(t)$, can be thought of coordinates of a two-dimensional phase space. As the motion of the pendulum evolves, the point given by (θ, ν) will move along a path in phase space. For different initial conditions, the motion will be described by different paths. Phase space plots can be divided into two categories: closed orbit or open orbit paths.

For the pendulum, closed orbit paths result when the pendulum is bound about the stable fixed point. Open orbit paths occur when there is a large enough angular velocity to cause the pendulum to go over the top.

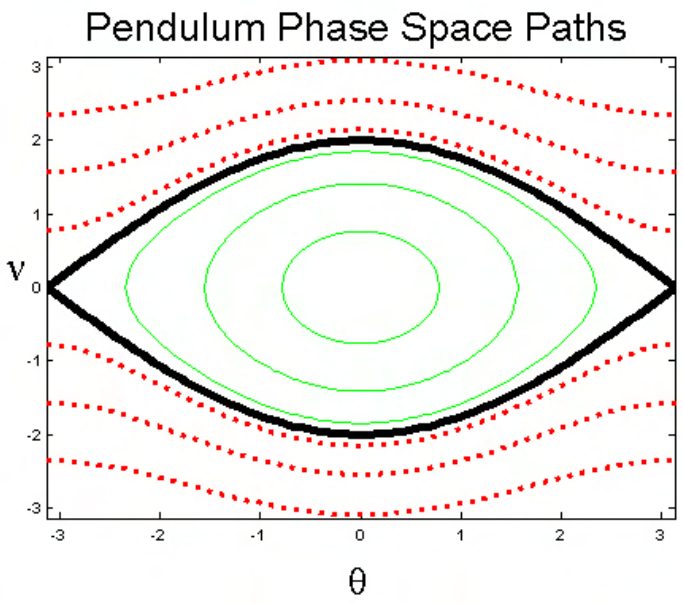

Figure 8. Various phase-space paths for a simple pendulum. The thin green curves are examples of closed orbits. The dotted red curves are examples of open orbits. The separatrix is the heavy dark curve.

Figure 8 illustrates the phase space paths of a simple pendulum for 10 different

initial conditions. The phase space paths are given by[5]

$$\nu^2 = \nu_o^2 + 2(\cos\theta - \cos\theta_o) \tag{III.33}$$

The separatrix is found when $\theta_o = \pi$ and $\nu_o = 0$ in Equation (III.33) giving us

$$\nu^2 = 2(\cos\theta + 1) \tag{III.34}$$

The separatrix separates locally bounded motion from locally unbounded motion and passes through the unstable fixed point $(\theta_o = \pi, \nu_o = 0)$.

Equation (III.32) is equivalent to the simple pendulum if $|a|$ and ϕ are constant, as is approximately the case for low gain in the FEL. The electron phase, ζ, can be viewed as the electron's position within an undulator period while a change in phase velocity is proportional to the electron's energy (recall $\dot{\nu} \propto \dot{\gamma}/\gamma$). The dimensionless optical field amplitude, $|a|$, is a measure of the field strength. A larger $|a|$ causes the phase space paths to evolve much faster (analogous to a larger $\sqrt{g/l}$ for the real pendulum). A larger $|a|$ also causes the separatrix to increase in size (along ν). The FEL separatrix is given by [13]:

$$\nu^2 = 2|a|[1 + \sin(\zeta + \phi)] \tag{III.35}$$

Figure 9 shows the evolution of 1000 electrons in phase space all with an initial $\nu_o = 0$ (on resonance) and $|a| = 1$. Notice that half the electrons gained energy from the optical field (increasing values of ν) and half the electrons lost energy to the optical field (decreasing values of ν). Notice how the electrons are becoming bunched along ζ. Since there are an equal number of electrons gaining and losing energy, the overall gain is zero. Gain is the fractional change in the power of the optical field

[5]Dimensionless pendulum equation given by $\overset{\circ\circ}{\theta} = -\sin\theta$. Multiply both sides by ν to get $\nu\,\overset{\circ}{\nu} = -\nu\sin\theta$, which is equivalent to $d[\nu^2/2 - \cos\theta]/dt = 0$, giving us Equation (III.33).

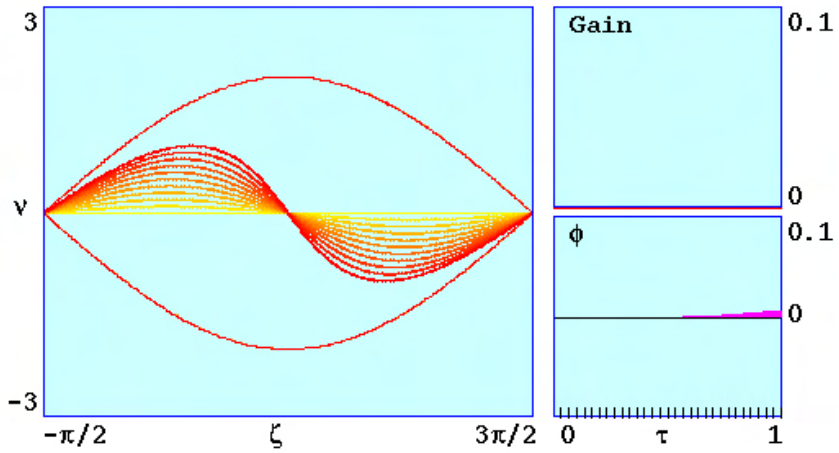

Figure 9. Phase space evolution for 1000 electrons with all with initial $\nu = 0$.

over a pass through the undulator. In symbols, we write:

$$G = \frac{P - P_o}{P_o} \tag{III.36}$$

and

$$P = |a|^2 \tag{III.37}$$

where the power, P is measured at the end of the undulator and P_o is the power at the beginning of the undulator. We will discuss gain in detail in the next section.

In Figure 10, we start out with an initial $\nu_o = 1.5$ and $|a| = 5.0$. There is an imbalance in the number of electrons that are gaining and losing energy from the optical field. In this particular case, there is a clear bunching of electrons near $\zeta = \pi$ resulting in gain.

B. ELECTRON BEAM AND OPTICAL FIELD INTERACTION

In the previous section, we derived the FEL pendulum equation which tells us the phase space evolution of electrons in an undulator period. Phase space evolutions that ended with good bunching at the appropriate phase resulted in gain (see Figure

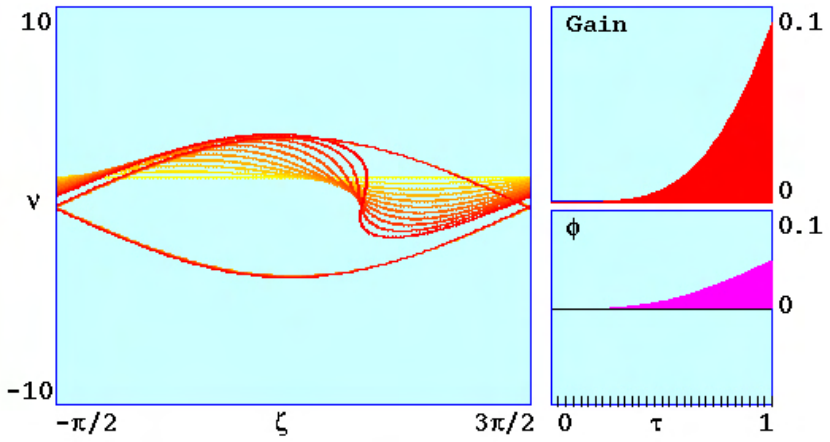

Figure 10. Phase space evolution for 1000 electrons all with initial $\nu = 1.5$.

10). The upper picture of Figure 11 illustrates bunching in an optical wavelength for

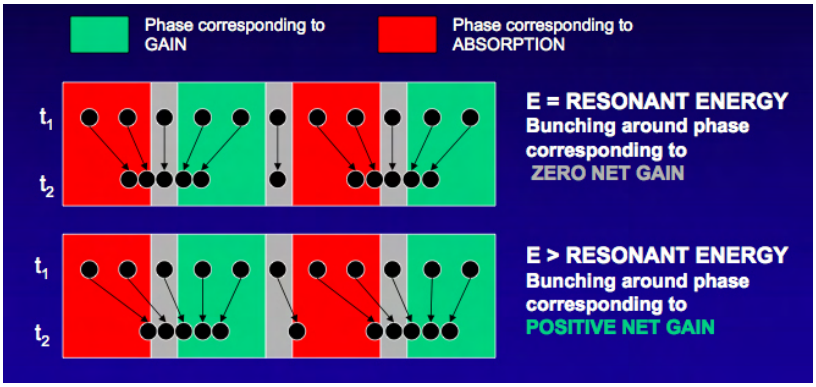

Figure 11. In the upper picture, electrons have an initial $\nu_o = 0$ which results in bunching but no gain. In the lower picture, electrons have a an initial $\nu_o > 0$ resulting in good bunching and positive gain from [4].

$\nu_o = 0$ or on-resonance case. At time t_1 the electrons start out evenly spaced within a section of the electron beam one wavelength of light long. At time t_2, the electrons' positions have evolved so that the number of electrons which give energy to the optical field (gain) equals the number of electrons which take energy from the optical field (absorption). The result is zero net gain but good bunching. In the lower picture, at

time t_1 evenly spaced electrons have an initial non-zero phase velocity, i.e. $\nu > 0$. At time t_2 the electrons' positions have evolved so that there are more electrons giving energy to the optical field than absorbing it. The result is positive gain, i.e., the optical field grows.

1. Maxwell's Equations

Let us quantitatively describe the interaction between the electron beam and the optical field. We begin with Maxwell's Equations in cgs units[6]:

$$\boldsymbol{\nabla} \cdot \mathbf{E} = 4\pi\rho \tag{III.38}$$

$$\boldsymbol{\nabla} \cdot \mathbf{B} = \mathbf{0} \tag{III.39}$$

$$\boldsymbol{\nabla} \times \mathbf{E} = -\frac{1}{c}\frac{\partial \mathbf{B}}{\partial t} \tag{III.40}$$

$$\boldsymbol{\nabla} \times \mathbf{B} = \frac{4\pi}{c}\mathbf{J} + \frac{1}{c}\frac{\partial \mathbf{E}}{\partial t} \tag{III.41}$$

where ρ is the charge density, $\mathbf{E}$ is the electric field, $\mathbf{B}$ is the magnetic field, and $\mathbf{J}$ is the current density. Equation (III.39) automatically implies that $\mathbf{B}$ is the curl of some other vector, $\mathbf{A}$, the magnetic vector potential[7]. We then have

$$\boldsymbol{\nabla} \cdot \mathbf{B} = \mathbf{0} \Rightarrow \mathbf{B} = \boldsymbol{\nabla} \times \mathbf{A} \tag{III.42}$$

If we substitute Equation (III.42) into Equation (III.40) we get

$$\boldsymbol{\nabla} \times \mathbf{E} = -\frac{1}{c}\frac{\partial}{\partial t}(\boldsymbol{\nabla} \times \mathbf{A})$$

$$\boldsymbol{\nabla} \times \mathbf{E} + \frac{1}{c}\frac{\partial}{\partial t}(\boldsymbol{\nabla} \times \mathbf{A}) = \mathbf{0}$$

$$\boldsymbol{\nabla} \times \left(\mathbf{E} + \frac{1}{c}\frac{\partial \mathbf{A}}{\partial t}\right) = \mathbf{0}$$

Recall from elementary vector calculus, if the curl of some vector is zero, then that vector is equal to minus the gradiant of a scalar[8], Φ, the electric potential. We can

[6] see [10], Chapters 6 and 11

[7] [14], Chapter 5

[8] Ibid

then write

$$\boldsymbol{\nabla} \times \left(\mathbf{E} + \frac{1}{c}\frac{\partial \mathbf{A}}{\partial t} \right) = \mathbf{0} \Rightarrow \mathbf{E} + \frac{1}{c}\frac{\partial \mathbf{A}}{\partial t} = -\boldsymbol{\nabla}\Phi$$

Therefore,

$$\mathbf{E} = -\boldsymbol{\nabla}\Phi - \frac{1}{c}\frac{\partial \mathbf{A}}{\partial t} \tag{III.43}$$

Equations (III.42) and (III.43) describe the electromagnetic radiation in terms of their potentials, $\mathbf{A}$ and Φ. If we substitute them into Equation (III.41) we arrive at[9]

$$\begin{aligned}
\boldsymbol{\nabla} \times \boldsymbol{\nabla} \times \mathbf{A} &= \frac{4\pi}{c}\mathbf{J} + \frac{1}{c}\frac{\partial}{\partial t}\left(-\boldsymbol{\nabla}\Phi - \frac{1}{c}\frac{\partial \mathbf{A}}{\partial t} \right) \\
\boldsymbol{\nabla}(\boldsymbol{\nabla} \cdot \mathbf{A}) - \boldsymbol{\nabla}^2\mathbf{A} &= \frac{4\pi}{c}\mathbf{J} - \frac{1}{c}\boldsymbol{\nabla}\left(\frac{\partial \Phi}{\partial t}\right) - \frac{1}{c^2}\frac{\partial^2 \mathbf{A}}{\partial t^2} \\
\boldsymbol{\nabla}^2\mathbf{A} - \frac{1}{c^2}\frac{\partial^2 \mathbf{A}}{\partial t^2} - \boldsymbol{\nabla}\left[\boldsymbol{\nabla} \cdot \mathbf{A} + \frac{1}{c}\frac{\partial \Phi}{\partial t} \right] &= -\frac{4\pi}{c}\mathbf{J}
\end{aligned} \tag{III.44}$$

For completeness, if we substitute Equation (III.43) into Equation (III.38) we get

$$\boldsymbol{\nabla} \cdot \left[-\boldsymbol{\nabla}\Phi - \frac{1}{c}\frac{\partial \mathbf{A}}{\partial t} \right] = 4\pi\rho$$

$$\boldsymbol{\nabla}^2\Phi + \frac{1}{c}\frac{\partial}{\partial t}(\boldsymbol{\nabla} \cdot \mathbf{A}) = -4\pi\rho \tag{III.45}$$

Equations (III.44) and (III.45) fully describes the optical field. By a judicious choice of Coulomb gauge, $\boldsymbol{\nabla} \cdot \mathbf{A} = 0$, Equation (III.44) becomes the full wave equation in terms of transverse current[10]

$$\boldsymbol{\nabla}^2\mathbf{A} - \frac{1}{c^2}\frac{\partial^2 \mathbf{A}}{\partial t^2} = -\frac{4\pi}{c}\mathbf{J}_\perp \tag{III.46}$$

We will use this equation to determine the electron beam to optical mode interaction.

2. FEL Wave Equation

For our helical undulator given by Equation (III.3), a solution to

$$\boldsymbol{\nabla}^2\mathbf{A} - \frac{1}{c^2}\frac{\partial^2 \mathbf{A}}{\partial t^2} = -\frac{4\pi}{c}\mathbf{J}_\perp \tag{III.47}$$

---

[9] Vector Identity 8, [14]

[10] [10], Chapter 6

can be written as

$$\mathbf{A}(\mathbf{x},t) = \frac{E(\mathbf{x},t)}{k}\hat{\boldsymbol{\epsilon}}e^{i\alpha} \tag{III.48}$$

where $E(\mathbf{x},t)$ is the complex optical amplitude, $\alpha = kz - \omega t$ is the carrier wave, $\hat{\boldsymbol{\imath}} = (-i,1,0)$ is optical field's polarization vector for circularly polarized light, and $\mathbf{x} = x\hat{\boldsymbol{\imath}} + y\hat{\boldsymbol{\jmath}} + z\hat{\mathbf{k}}$ is the position vector. Substituting Equation (III.48) into (III.47), we get the following

$$\frac{\partial^2\mathbf{A}}{\partial x^2} = \frac{\hat{\boldsymbol{\epsilon}}e^{i\alpha}}{k}\frac{\partial^2 E}{\partial x^2} \tag{III.49}$$

$$\frac{\partial^2\mathbf{A}}{\partial y^2} = \frac{\hat{\boldsymbol{\epsilon}}e^{i\alpha}}{k}\frac{\partial^2 E}{\partial y^2} \tag{III.50}$$

$$\frac{\partial^2\mathbf{A}}{\partial z^2} = \frac{\hat{\boldsymbol{\epsilon}}e^{i\alpha}}{k}\left[\frac{\partial^2 E}{\partial z^2} + 2ik\frac{\partial E}{\partial z} - k^2 E\right] \tag{III.51}$$

$$\frac{\partial^2\mathbf{A}}{\partial t^2} = \frac{\hat{\boldsymbol{\epsilon}}e^{i\alpha}}{k}\left[\frac{\partial^2 E}{\partial t^2} - 2i\omega\frac{\partial E}{\partial t} - \omega^2 E\right] \tag{III.52}$$

For a laser beam, we can make a few simplifications. If we assume that optical wave amplitude and phase are slowly varying along the z axis, second derivatives in z and t can be dropped compared to first derivatives. Substituting these back into Equation (III.47) and using $\omega = kc$, we arrive at

$$\frac{\hat{\boldsymbol{\epsilon}}e^{i\alpha}}{k}\left[\boldsymbol{\nabla}_{\perp}^{\mathbf{2}} + 2ik\left(\frac{\partial}{\partial z} + \frac{1}{c}\frac{\partial}{\partial t}\right)\right]E = -\frac{4\pi}{c}\mathbf{J}_{\perp} \tag{III.53}$$

where $\boldsymbol{\nabla}_{\perp}^{\mathbf{2}} = \partial^2/\partial x^2 + \partial^2/\partial y^2$ is the transverse Laplacian operator. We can simplify the expression further by a change of coordinates, $u = z - ct$, which follows the light[11], and recalling dimensionless time, $\tau = ct/L$, then

$$\begin{aligned}
\frac{\partial}{\partial z} &= \frac{\partial u}{\partial z}\frac{\partial}{\partial u} + \frac{\partial \tau}{\partial z}\frac{\partial}{\partial \tau} = \frac{\partial}{\partial u} \\
\frac{\partial}{\partial t} &= \frac{\partial \tau}{\partial t}\frac{\partial}{\partial \tau} + \frac{\partial u}{\partial t}\frac{\partial}{\partial u} = \frac{c}{L}\frac{\partial}{\partial \tau} - c\frac{\partial}{\partial u} \\
\text{so that, } \frac{\partial}{\partial z} + \frac{1}{c}\frac{\partial}{\partial t} &= \frac{\partial}{\partial u} + \frac{1}{c}\left[\frac{c}{L}\frac{\partial}{\partial \tau} - c\frac{\partial}{\partial u}\right] \\
&= \frac{1}{L}\frac{\partial}{\partial \tau}
\end{aligned} \tag{III.54}$$

[11] Coordinate transformation is also known as method of characteristics. See [15]

We have effectively collapsed z and t into one variable τ. Multiplying Equation (III.53) by $k\hat{\boldsymbol{\epsilon}}^* e^{i\alpha}$, making use of Equation (III.54), and $\hat{\boldsymbol{\epsilon}}^* \cdot \hat{\boldsymbol{\epsilon}} = 2$, we now have

$$\left[\boldsymbol{\nabla}_{\perp}^{\mathbf{2}} + 2ik\left(\frac{1}{L}\frac{\partial}{\partial\tau}\right)\right] E = -2\pi\frac{k}{c}e^{-i\alpha}\mathbf{J}_{\perp}\cdot\hat{\boldsymbol{\epsilon}}^* \tag{III.55}$$

We can express the electron current density as a sum over all electrons

$$\mathbf{J}_{\perp} = -ec\sum_i \boldsymbol{\beta}_{\perp}\delta^{(3)}(\mathbf{x} - \mathbf{x_i}(t)) \tag{III.56}$$

where e is the magnitude of electron's charge, $\mathbf{x_i}$ is the electron's position at time t, and $\delta^{(3)}$ is the three-dimensional delta-function. Equation (III.11), $\boldsymbol{\beta}_{\perp}$, can also be expressed as

$$\boldsymbol{\beta}_{\perp} = \Re\{-\frac{K}{\gamma}i\hat{\boldsymbol{\epsilon}}e^{-ik_o z}\} \tag{III.57}$$

where $\Re$ signifies taking the real part of the complex argument. Combining these equations, Equation (III.55) becomes

$$\left[\boldsymbol{\nabla}_{\perp}^{\mathbf{2}} + 2ik\left(\frac{1}{L}\frac{\partial}{\partial\tau}\right)\right] E(\mathbf{r},\tau) = -4\pi ikeK\rho < \frac{e^{-i\zeta}}{\gamma} > \tag{III.58}$$

where $\mathbf{r} = x\hat{i} + y\hat{j}$. We have made use of Equation (III.14) and

$$\rho(\mathbf{x},t) = \int_V \sum_i \delta^{(3)}(\mathbf{x} - \mathbf{x_i}(t))dV \tag{III.59}$$

The average $< ... >$ represents an average over sample electrons in a volume element. If we multiply Equation (III.58) by $-4\pi iNeKL^2/\gamma^2 mc^2 k$, recall the dimensionless optical field amplitude, $|a| = 4\pi NeK|E|L/\gamma^2 mc^2$, and define a dimensionless current density $j = 8\pi^2 Ne^2K^2L^2\rho/\gamma^3 mc^2$, we have

$$\left[-\frac{iL}{2k}\boldsymbol{\nabla}_{\perp}^{\mathbf{2}} + \frac{\partial}{\partial\tau}\right] a(\mathbf{r},\tau) =< -je^{-i\zeta} > \tag{III.60}$$

when $\gamma \approx \gamma_o$, a reasonable assumption for all the electrons during the length of the interaction. Looking at the factors multiplying the transverse Laplacian suggests we define dimensionless transverse coordinates (where the tildes refer to the dimensionless

variables):

$$\tilde{x} = x\sqrt{\frac{k}{2L}} \tag{III.61}$$

$$\tilde{y} = y\sqrt{\frac{k}{2L}} \tag{III.62}$$

We can now recast the Laplacian operator into a dimensionless Laplacian operator, $\tilde{\boldsymbol{\nabla}}^{\mathbf{2}}_{\perp}$, since

$$\frac{\partial^2}{\partial x^2} + \frac{\partial^2}{\partial y^2} = \frac{k}{2L}\left[\frac{\partial^2}{\partial \tilde{x}^2} + \frac{\partial^2}{\partial \tilde{y}^2}\right] \tag{III.63}$$

The FEL wave equation now becomes,

$$\left[-\frac{i}{4}\tilde{\boldsymbol{\nabla}}^{\mathbf{2}}_{\perp} + \frac{\partial}{\partial \tau}\right] a(\tilde{\mathbf{r}}, \tau) = < -je^{-i\zeta} > \tag{III.64}$$

where $a(\tilde{\mathbf{r}}, \tau) = |a|e^{i\phi}$, the complex dimensionless optical field amplitude, measures the optical field strength in the interaction region; the dimensionless current j measures the interaction between the electron beam and the optical mode; and $< e^{-i\zeta} >$ measures the amount of electron bunching. If j is large ($j >> \pi$), the optical field a changes rapidly so we have high gain. If j is small ($j << \pi$), we have low gain.

3. Gain

Thus far in our development of FEL physics, we have studied free electrons interacting with laser light through a Lorentz force interaction in the undulator. We have described, through the pendulum equation, the process of physically bunching the electrons in phase space leading to coherent radiation. Finally, we have coupled this radiation, through Maxwell's equations, with the electron beam co-propagating in the undulator with the optical beam (see Equation (III.64)).

We must now discuss the modification of the field by FEL amplification. In weak fields, $|a| << \pi$ and low gain $j << \pi$, we can apply a perturbation expansion of the pendulum equation resulting in an expression for optical mode amplication [13]

$$G(\tau) = jF\left(\frac{2 - 2\cos(\nu_o\tau) - \nu_o\tau\sin(\nu_o\tau)}{\nu_o^3}\right) \tag{III.65}$$

where the filling factor, F, is the ratio of areas of the electron beam to the optical mode. Gain is proportional to the dimensionless current density, j. At $\tau = 1$, the final gain is

$$G(1) = jF\left(\frac{2 - 2\cos(\nu_o) - \nu_o \sin(\nu_o)}{\nu_o^3}\right) \tag{III.66}$$

Equation (III.66) is shown in Figure 12. Notice the anti-symmetric nature in ν_o

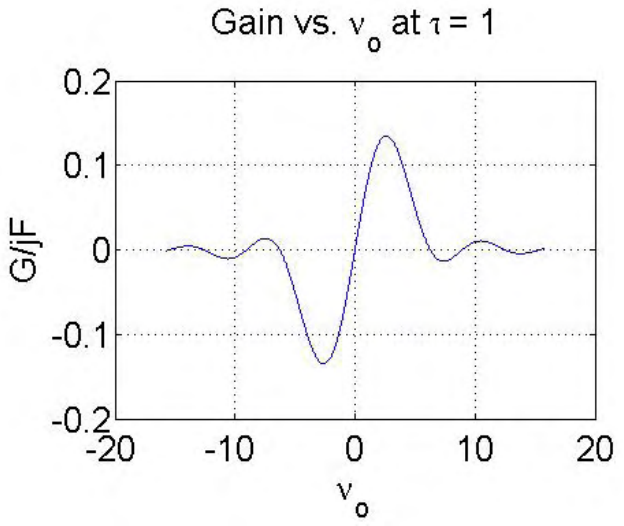

Figure 12. Gain curve plotted at $\tau = 1$.

and zero gain at $\nu_o = 0$. The gain peaks at $\nu_o \approx 2.6$ with peak absorption at $\nu_o \approx -2.6$. When the electrons are at phase velocities slightly above resonance, the amount of energy transferred from the electron beam to the optical mode is maximized meaning that the optical mode is amplified by the electron beam. In an operating FEL, electrons that initially go through the undulator spontaneously emit in a spectrum (Figure 13a) centered around the resonant frequency. The weak field low gain curve (Figure 13b) narrows the spectrum over many passes (Figure 13c). Over many passes, the laser spectrum narrows due to mode competition. The top of Figure 13d shows a narrow linewidth after 2500 passes requiring only a few microseconds of FEL operation.

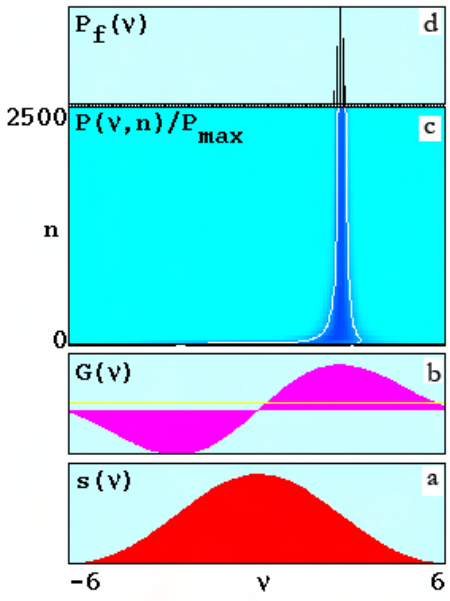

Figure 13. FEL coherence as it evolves from a broadband spectrum.(a) Broadband spectrum from spontaneous emission. (b) Low field gain curve. (c) Narrowing broadband spectrum over many passes. (d) Final power spectrum showing narrow linewidth.

IV. OPTICAL THEORY

In the previous section, we described how oscillating electrons co-propagating with the optical field gave rise to amplified laser light. We will now restrict our discussion to the the laser light itself as it propagates from the interaction region in free space. We are interested in the transverse optical mode structure because the burn pattern ($\propto |a(\tilde{x},\tilde{y})|^2$) will determine the intensity delivered to a beam optic or a target. Free electron lasers (FEL) primarily operate in the fundamental Gaussian mode, but a few higher-order modes are also possible. It has been shown in simulations and experiments that a few higher order modes can develop when the FEL is operated with mirror shifts and tilts, electron beam shifts or mirror asymmetry. Building on previous work [5], we will develop the mathematics for Hermite-Gaussian modes and a means of finding the coefficients for a given waveform. The modal analysis described here will be applied to FEL mirror distortions which is being investigated for the first time.

A. OPTICAL WAVE EQUATION

We first begin our discussion of optical theory by describing light propagation when no sources are present. Recall from the previous chapter, the FEL wave equation in the undulator is

$$\left[-\frac{i}{4}\tilde{\boldsymbol{\nabla}}_{\perp}^{\mathbf{2}} + \frac{\partial}{\partial\tau}\right] a(\tilde{\mathbf{r}},\tau) =< -je^{-i\zeta} > \tag{IV.1}$$

when no sources are present, i.e., $j = 0$ and Equation (IV.1), reduces to

$$\left[\tilde{\boldsymbol{\nabla}}_{\perp}^{\mathbf{2}} + 4i\frac{\partial}{\partial\tau}\right] a(\tilde{\mathbf{r}},\tau) = 0 \tag{IV.2}$$

where $a = |a|e^{i\phi}$, the complex dimensionless field amplitude, measures the optical field strength. In terms of the FEL system, the following description is applicable outside of the undulator or when the electron current is zero inside the undulator. In our definitions of dimensionless variables $\tilde{x}$, $\tilde{y}$, and τ, L represented the length of

the undulator. It will now represent the length that the optical mode travels. Our task now will be to find solutions of Equation (IV.2) to investigate transverse mode properties.

B. FUNDAMENTAL MODE

A form for the solution of Equation (IV.2) in lowest order can be written down as

$$a(\tilde{\mathbf{r}},\tau) = a_o e^{-\left(p(\tau)+\frac{\tilde{r}^2}{\tilde{z}_o\, q(\tau)}\right)} \tag{IV.3}$$

where $a(\tilde{\mathbf{r}},\tau)$ is the dimensionless complex field amplitude proportional to the electric field, $\tilde{r}^2 = \tilde{x}^2 + \tilde{y}^2$, and a_o is the real dimensionless optical amplitude at $\tilde{x} = 0, \tilde{y} = 0, \tau = 0$. Functions $p(\tau)$ and $q(\tau)$ are yet to be determined. Rayleigh length, $\tilde{z}_o = Z_o/L$, is the longitudinal distance from the mode waist at which the optical area doubles, i.e., where the mode radius exceeds the value at the waist by a factor of $\sqrt{2}$. It is a measure of how the optical mode expands (see Figure 14). Equation (IV.3)

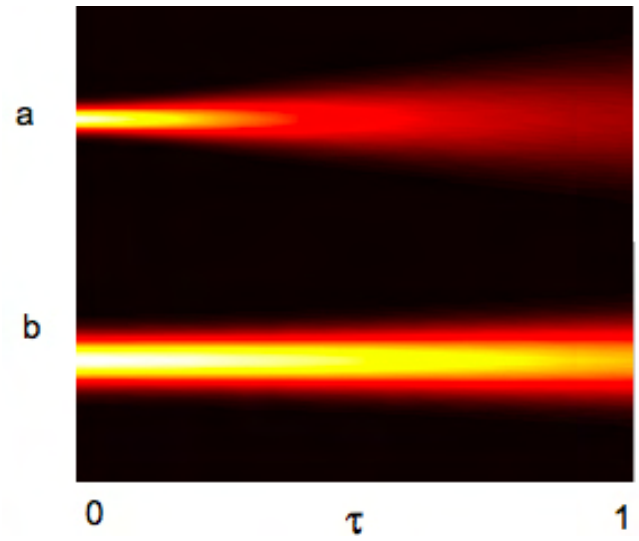

Figure 14. Cross section of a Gaussian mode propagating from $\tau = 0 \rightarrow 1$. The mode with a smaller Rayleigh length expands more quickly. (a) $\tilde{z}_o = 0.20$, $\tau_w = 0.0$ (b) $\tilde{z}_o = 0.8$, $\tau_w = 0.0$

is the dimensionless analogue of a form used by [16], *et al.* Since we are solving a second-order differential equation, we must specify initial conditions to determine a unique solution. We stipulate that at $\tau = 0$, $a(\tilde{\mathbf{r}}, 0) = a_o e^{-\frac{\tilde{r}^2}{\tilde{z}_o}}$, an initially transverse Gaussian wavefront. The initial conditions then require:

$$\begin{aligned} p(0) &= 0 \\ q(0) &= 1 \end{aligned} \tag{IV.4}$$

Our job will be to find $p(\tau)$ and $q(\tau)$.

We now take derivatives of Equation (IV.3) resulting in:

$$\frac{\partial^2 a}{\partial \tilde{x}^2} = \left(\frac{-2}{\tilde{z}_o q} + \frac{4\tilde{x}^2}{\tilde{z}_o^2 q^2} \right) a \tag{IV.5}$$

$$\frac{\partial^2 a}{\partial \tilde{y}^2} = \left(\frac{-2}{\tilde{z}_o q} + \frac{4\tilde{y}^2}{\tilde{z}_o^2 q^2} \right) a \tag{IV.6}$$

$$\frac{\partial a}{\partial \tau} = \left(-\overset{\circ}{p} + \frac{\tilde{x}^2 \overset{\circ}{q}}{\tilde{z}_o q^2} + \frac{\tilde{y}^2 \overset{\circ}{q}}{\tilde{z}_o q^2} \right) a \tag{IV.7}$$

(Recall $(\overset{\circ}{.}) = d(\ldots)/d\tau$.) Combining Equations (IV.5), (IV.6), (IV.7) into (IV.2) and dividing through by a, we are arrive at

$$-\frac{2}{\tilde{z}_o q} + \frac{4\tilde{x}^2}{\tilde{z}_o^2 q^2} - \frac{2}{\tilde{z}_o q} + \frac{4\tilde{y}^2}{\tilde{z}_o^2 q^2} + 4i \left(-\overset{\circ}{p} + \frac{\tilde{x}^2 \overset{\circ}{q}}{\tilde{z}_o q^2} + \frac{\tilde{y}^2 \overset{\circ}{q}}{\tilde{z}_o q^2} \right) = 0 \tag{IV.8}$$

Making use of $\tilde{r}^2 = \tilde{x}^2 + \tilde{y}^2$, we have

$$\frac{\tilde{r}^2}{\tilde{z}_o q^2} \left(\frac{1}{\tilde{z}_o} + i \overset{\circ}{q} \right) = \left(\frac{1}{\tilde{z}_o q} + i \overset{\circ}{p} \right) \tag{IV.9}$$

For this equation to hold for any $\tilde{r}^2$ at some particular time τ, both terms in parentheses must be identically zero. Solving the left hand side for $q(\tau)$

$$\begin{aligned} \overset{\circ}{q} &= \frac{i}{\tilde{z}_o} \\ q(\tau) &= \int^{\tau} \frac{i}{\tilde{z}_o} d\tau' \\ &= q_o + \frac{i\tau}{\tilde{z}_o} \end{aligned} \tag{IV.10}$$

Applying the initial conditions, Equation (IV.4), we find

$$q(\tau) = 1 + \frac{i\tau}{\tilde{z}_o} \tag{IV.11}$$

Solving the right hand side of Equation (IV.9) for $p(\tau)$ and substituting Equation (IV.11), we find $\overset{\circ}{p}(\tau)$ to be

$$\overset{\circ}{p} = \frac{i\tilde{z}_o}{\tilde{z}_o^2 + \tau^2} + \frac{\tau}{\tilde{z}_o^2 + \tau^2} \tag{IV.12}$$

Integrating with respect to τ and applying initial conditions, we have

$$p(\tau) = \int^{\tau} \left(\frac{i\tilde{z}_o}{\tilde{z}_o^2 + \tau'^2} + \frac{\tau'}{\tilde{z}_o^2 + \tau'^2}\right) d\tau' \tag{IV.13}$$

$$p(\tau) = i \arctan \frac{\tau}{\tilde{z}_o} + \ln \sqrt{\frac{\tau^2 + \tilde{z}_o^2}{\tilde{z}_o^2}} \tag{IV.14}$$

Substituting Equations (IV.11) and (IV.14) back into Equation (IV.3), we find

$$a(\tilde{\mathbf{r}}, \tau) = a_o e^{\left(-i \arctan \frac{\tau}{\tilde{z}_o} - \ln \sqrt{\frac{\tau^2 + \tilde{z}_o^2}{\tilde{z}_o^2}}\right)} e^{\left(-\frac{\tilde{r}^2}{\tilde{z}_o(1 + \frac{i\tau}{\tilde{z}_o})}\right)} \tag{IV.15}$$

We can clean up this mess if we make a few substitutions. From Equation (IV.11), we have

$$\begin{aligned} \frac{1}{q(\tau)} &= \frac{1}{1 + \frac{i\tau}{\tilde{z}_o}} \\ &= \frac{\tilde{z}_o}{\tilde{z}_o + \frac{\tau^2}{\tilde{z}_o}} - i\frac{\tau}{\tilde{z}_o + \frac{\tau^2}{\tilde{z}_o}} \end{aligned} \tag{IV.16}$$

With the benefit of hindsight, we can make the following definition:

$$\begin{aligned} \tilde{w}^2(\tau) &= \tilde{z}_o + \frac{\tau^2}{\tilde{z}_o} \\ \tilde{w}(\tau) &= \sqrt{\tilde{z}_o + \frac{\tau^2}{\tilde{z}_o}} \end{aligned} \tag{IV.17}$$

Equation (IV.17) represents the optical mode radius as shown in Figure 15. The term $\tilde{z}_o$ is the dimensionless analogue of the dimesional Rayleigh length. The derivation has assumed that the beam waist occurs at $\tau = 0$, that is, $\tilde{w}(0) = \tilde{w}_o = \sqrt{\tilde{z}_o}$. But

the beam waist may be positioned anywhere along τ. It is a trivial matter to make a time translation in the equations such that, $\tau \rightarrow (\tau - \tau_w)$. With Equation (IV.17), we can re-express $1/q$ in terms of w and w_o. Equation (IV.16) now becomes

$$\frac{1}{q(\tau)} = \frac{\tilde{w}_o^2}{\tilde{w}^2(\tau)} - i\frac{\tau}{\tilde{w}^2(\tau)} \tag{IV.18}$$

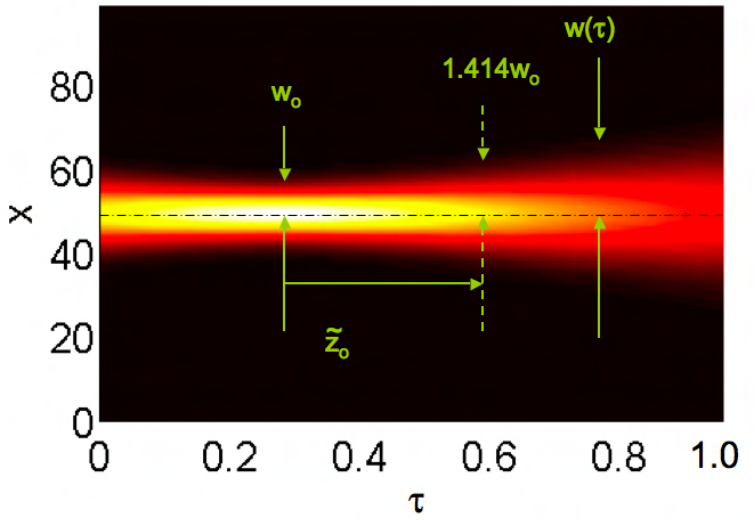

Figure 15. Cross section of a Gaussian mode as it propagates from $\tau = 0 \rightarrow 1$ illustrating the optical mode radius. $\tau_w = 0.3$, $\tilde{z}_o = 0.3$

Returning to Equation (IV.15) and substituting Equation (IV.18), the optical field becomes[1]

$$a(\tilde{\mathbf{r}}, \tau) = a_o \frac{\tilde{w}_o}{\tilde{w}(\tau)} e^{-\frac{\tilde{r}^2}{\tilde{w}^2(\tau)}} e^{i\frac{\tilde{r}^2\tau}{\tilde{w}_o^2\tilde{w}^2(\tau)}} e^{-i\arctan\frac{\tau}{\tilde{z}_o}} \tag{IV.19}$$

Finally, we can write down the fundamental mode of the optical field as

$$a(\tilde{\mathbf{r}}, \tau) = \overbrace{a_o \frac{\tilde{w}_o}{\tilde{w}(\tau)} e^{-\frac{\tilde{r}^2}{\tilde{w}^2(\tau)}}}^{\text{Amplitude}} \underbrace{e^{i\left(\frac{\tilde{r}^2\tau}{\tilde{w}_o^2\tilde{w}^2(\tau)} - \arctan\frac{\tau}{\tilde{z}_o}\right)}}_{\text{Phase}} \tag{IV.20}$$

[1]The square root term can be expressed more compactly as $\tilde{w}_o/\tilde{w}$

where the mode waist is at $\tau_w = 0$. For any arbitrary location of the mode waist, we have

$$a(\tilde{\mathbf{r}}, \tau) = \overbrace{a_o \frac{\tilde{w}_o}{\tilde{w}(\tau - \tau_w)} e^{-\frac{\tilde{r}^2}{\tilde{w}^2(\tau-\tau_w)}}}^{\text{Amplitude}} \underbrace{e^{i\left(\frac{\tilde{r}^2(\tau-\tau_w)}{\tilde{w}_o^2 \tilde{w}^2(\tau-\tau_w)} - \arctan\frac{\tau-\tau_w}{\tilde{z}_o}\right)}}_{\text{Phase}} \tag{IV.21}$$

As can be seen, the amplitude falls off as $e^{-\tilde{r}^2/\tilde{w}^2}$ and is clearly Gaussian while the phase term includes both $\tilde{r}$ and τ dependence. Equations (IV.20) and (IV.21) represents the lowest-order transverse electromagnetic mode. Figure 16 shows the surface

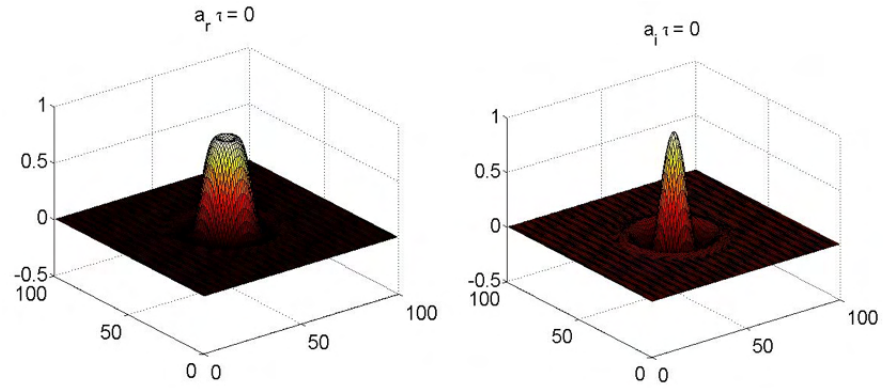

Figure 16. Real and imaginary parts of complex Gaussian mode at $\tau = 0$ with $\tau_w = 0.5$.

plots of the real and imaginary parts of Equation (IV.21). The real and imaginary parts of $a(\tilde{\mathbf{r}}, \tau)$ provides us with the amplitude and phase of the optical field since

$$|a(\tilde{\mathbf{r}}, \tau)| = \sqrt{\Re\{a\}^2 + \Im\{a\}^2} \tag{IV.22}$$

and

$$\phi(\tilde{\mathbf{r}}, \tau) = \arctan \frac{\Im\{a\}}{\Re\{a\}} \tag{IV.23}$$

where ϕ is the optical phase. Burn patterns are recognizable through the power in the optical field, i.e., the optical field amplitude squared. In the following discussions we

will only plot the amplitude of the mode instead of the power (or amplitude squared) because we would lose detail in the plots.

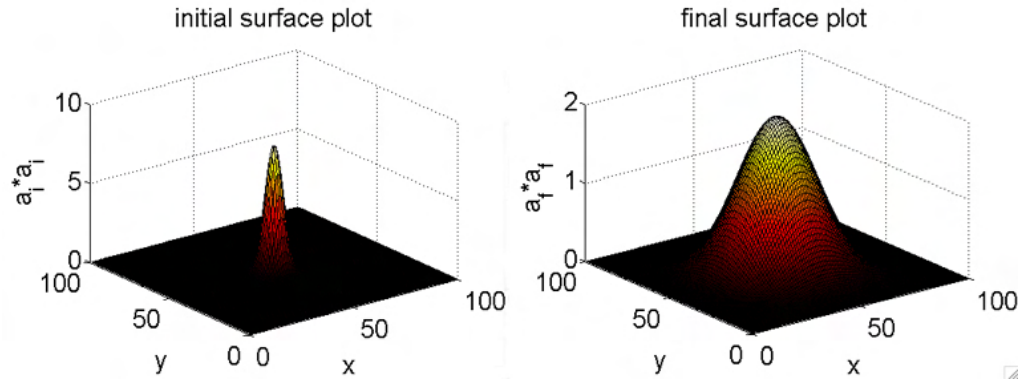

Figure 17. Initial ($\tau = 0$) and final ($\tau = 1$) surface amplitudes for the lowest order mode where yellow represents highest largest amplitude.

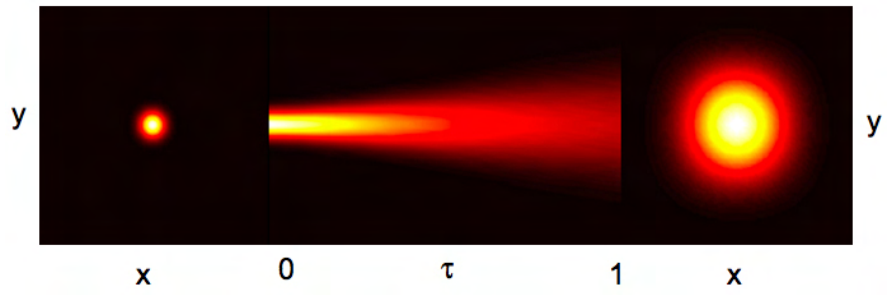

Figure 18. Three panels shows cross sections of a Gaussian mode as it propagates from $\tau = 0 \rightarrow 1$. $\tilde{z}_o = 0.25$ $\tau_w = 0$.

Figure 17 is a surface plot for a Gaussian mode at $\tau = 0$ and $\tau = 1$. Figure 18 is composed of three panels. The first panel shows a cross section ($\tilde{x}$ vs. $\tilde{y}$) of the Gaussian mode at $\tau = 0$. The middle panel shows a cross section ($\tilde{y}$ vs. τ) as the mode propagates. The last panel shows the cross section of the mode at $\tau = 1$ ($\tilde{x}$ vs. $\tilde{y}$). Notice how a small Rayleigh length has spread the mode considerably.

C. HIGHER ORDER MODES

In order to account for more complicated variations along transverse directions, we can generalize the trial solution Equation (IV.3):

$$a(\tilde{\mathbf{r}},\tau) = a_o g\left(\frac{\tilde{x}}{\tilde{w}(\tau)}\right) h\left(\frac{\tilde{y}}{\tilde{w}(\tau)}\right) e^{-(p(\tau)+\frac{\tilde{r}^2}{\tilde{z}_o q(\tau)})} \tag{IV.24}$$

The functions g and h will allow for a more intricate variance along transverse directions. Again, we demand the same initial conditions, namely, $a(\tilde{\mathbf{r}},0) = a_o e^{-\frac{\tilde{r}^2}{\tilde{z}_o}}$. This implies, $p(0) = 0$, $q(0) = 1$, and $g(\tilde{x}/\tilde{w}_o) = h(\tilde{y}/\tilde{w}_o) = 1$ since the initial Gaussian form already expressed in the factor $e^{\tilde{r}^2/\tilde{z}_o}$. As before, our job now will be to find the unknown functions, $p(\tau)$, $q(\tau)$, $g(\tilde{x}/\tilde{w}(\tau))$, and $h(\tilde{y}/\tilde{w}(\tau))$ at later times. But before we begin taking derivatives, let us consider derivatives of g (and by analogy h) to illustrate the chain rule:

$$\begin{aligned}\frac{\partial g}{\partial \tilde{x}} &= \frac{\partial g}{\partial(\frac{\tilde{x}}{\tilde{w}})}\frac{\partial}{\partial \tilde{x}}\left(\frac{\tilde{x}}{\tilde{w}}\right) \\ &= \frac{1}{\tilde{w}}\frac{\partial g}{\partial(\frac{\tilde{x}}{\tilde{w}})} \\ &= \frac{1}{\tilde{w}}g' \end{aligned} \tag{IV.25}$$

$$\begin{aligned}\frac{\partial^2 g}{\partial \tilde{x}^2} &= \frac{\partial}{\partial \tilde{x}}\frac{\partial g_1}{\partial \tilde{x}} \\ &= \frac{1}{\tilde{w}^2}g'' \end{aligned} \tag{IV.26}$$

and

$$\begin{aligned}\frac{\partial g}{\partial \tau} &= \frac{\partial g}{\partial(\frac{\tilde{x}}{\tilde{w}})}\frac{\partial}{\partial \tau}\left(\frac{x}{\tilde{w}}\right) \\ &= \tilde{x}\frac{\partial g}{\partial(\frac{\tilde{x}}{\tilde{w}})}\left(-\frac{1}{\tilde{w}^2}\right)\frac{\partial \tilde{w}}{\partial \tau} \\ &= -\frac{\tilde{x}}{\tilde{w}^2}g'\ \mathring{\tilde{w}} \end{aligned} \tag{IV.27}$$

As you can see, the primes over g denote a derivative with respect to its argument. This little fact will become handy later. Taking derivatives of Equation (IV.24) results in:

$$\frac{\partial^2 a}{\partial \tilde{x}^2} = a_o \left[\frac{1}{\tilde{w}^2} g'' h - \frac{4 g' h \tilde{x}}{\tilde{w} \tilde{z}_o q} - \frac{2gh}{\tilde{z}_o q} + \frac{4gh\tilde{x}^2}{\tilde{z}_o^2 q^2} \right] e^{-(p(\tau) + \frac{\tilde{r}^2}{\tilde{z}_o q(\tau)})} \tag{IV.28}$$

$$\frac{\partial^2 a}{\partial \tilde{y}^2} = a_o \left[\frac{1}{\tilde{w}^2} g h'' - \frac{4 g h' \tilde{y}}{\tilde{w} \tilde{z}_o q} - \frac{2gh}{\tilde{z}_o q} + \frac{4gh\tilde{y}^2}{\tilde{z}_o^2 q^2} \right] e^{-(p(\tau) + \frac{\tilde{r}^2}{\tilde{z}_o q(\tau)})} \tag{IV.29}$$

$$\frac{\partial a}{\partial \tau} = a_o \left[-\frac{1}{\tilde{w}^2} g' h \overset{\circ}{\tilde{w}} \tilde{x} - \frac{1}{\tilde{w}^2} g h' \overset{\circ}{\tilde{w}} \tilde{y} - gh \overset{\circ}{p} + \frac{gh\tilde{x}^2}{\tilde{z}_o q^2} \overset{\circ}{q} + \frac{gh\tilde{y}^2}{\tilde{z}_o q^2} \overset{\circ}{q} \right] e^{-(p(\tau) + \frac{\tilde{r}^2}{\tilde{z}_o q(\tau)})} \tag{IV.30}$$

Substituting Equations (IV.28), (IV.29), and (IV.30) into (IV.2), and dividing through by $a_o g h e^{-(p(\tau) + \frac{\tilde{r}^2}{\tilde{z}_o q(\tau)})}$, we have the following unpleasant monster:

$$\underbrace{\frac{1}{\tilde{w}^2}\frac{g''}{g} - \frac{4\tilde{x}}{\tilde{w}\tilde{z}_o q}\frac{g'}{g} - 4i\frac{\overset{\circ}{\tilde{w}}}{\tilde{w}^2}\tilde{x}\frac{g'}{g}}_{\tilde{x} \text{ only}} + \underbrace{\frac{1}{\tilde{w}^2}\frac{h''}{h} - \frac{4\tilde{y}}{\tilde{w}\tilde{z}_o q}\frac{h'}{h} - 4i\frac{\overset{\circ}{\tilde{w}}}{\tilde{w}^2}\tilde{y}\frac{h'}{h}}_{\tilde{y} \text{ only}} +$$

$$\underbrace{+\tilde{r}^2\left(\frac{4}{\tilde{z}_o^2 q^2} + \frac{4i}{\tilde{z}_o q^2}\overset{\circ}{q}\right)}_{\tilde{r}^2 \text{ only}} \quad \underbrace{-\frac{4}{\tilde{z}_o q} - 4i\overset{\circ}{p}}_{\text{no } \tilde{r} \text{ dependence}} \quad = \quad 0 \tag{IV.31}$$

In order for Equation (IV.31) to have a solution at a given time τ (i.e. a transverse plane), the $\tilde{x}$ dependent terms should equal a constant, let's say, $-\alpha$. The $\tilde{y}$ dependent terms should equal another constant, let's say $-\beta$. The $\tilde{r}^2$ dependent terms should be identically zero since it must be valid for at any location in the transverse plane. Finally, the terms that don't depend on $\tilde{r}$, should equal $\alpha + \beta$, so that the left hand side sums to zero. Solving the $\tilde{r}$ equation, we have

$$\tilde{r}^2\left(\frac{4}{\tilde{z}_o^2 q^2} + \frac{4i}{\tilde{z}_o q^2}\overset{\circ}{q}\right) = 0 \tag{IV.32}$$

$$\frac{4\tilde{r}^2}{\tilde{z}_o q^2}\left[\frac{1}{\tilde{z}_o} + i\overset{\circ}{q}\right] = 0 \tag{IV.33}$$

For this equation to hold for any $\tilde{r}$, the term in bracket must be identically zero. But we have seen this requirement before in the fundamental mode derivation. Applying

the initial conditions, we find that

$$q(\tau) = 1 + \frac{i\tau}{\tilde{z}_o} \tag{IV.34}$$

Returning to the $\tilde{x}$ dependence of Equation (IV.31), we multiply through by $g\tilde{w}^2$ and collect terms in derivatives of g, giving us

$$g'' - 4\tilde{x}\left(\frac{\tilde{w}}{\tilde{z}_o q} + i\,\overset{\circ}{\tilde{w}}\right) g' + \alpha\tilde{w}^2 g = 0 \tag{IV.35}$$

Let us evaluate the parenthetical term, recalling Equations (IV.17), (IV.18), and noting that $\overset{\circ}{\tilde{w}} = \tau/\tilde{w}_o^2\tilde{w}$, we find

$$\begin{aligned}\left(\frac{\tilde{w}}{\tilde{z}_o q} + i\,\overset{\circ}{\tilde{w}}\right) &= \frac{\tilde{w}}{\tilde{w}_o^2}\left(\frac{\tilde{w}_o^2}{\tilde{w}^2} - i\frac{\tau}{\tilde{w}^2}\right) + i\frac{\tau}{\tilde{w}_o^2\tilde{w}} \\ &= \frac{1}{\tilde{w}}\end{aligned} \tag{IV.36}$$

So now we have

$$g'' - \frac{4x}{\tilde{w}} g' + \alpha\tilde{w}^2 g = 0 \tag{IV.37}$$

The above equation is close to the form of the Hermite equation [12], $y'' - 2xy' + \lambda y = 0$. Recall that the primes denote a derivative with respect to the argument of the function. So a judicious change in variables will allow us to recast Equation (IV.37) in precisely the form of Hermite's equation. Let

$$\xi = \frac{\sqrt{2}\tilde{x}}{\tilde{w}} \rightarrow \tilde{x} = \frac{\tilde{w}\xi}{\sqrt{2}} \tag{IV.38}$$

$$\partial\xi = \sqrt{2}\partial(\frac{\tilde{x}}{\tilde{w}}) \tag{IV.39}$$

Using Equations (IV.38) and (IV.39) on (IV.37), results in

$$\frac{\partial g^2}{\partial\xi^2} - 2\xi\frac{\partial g}{\partial\xi} + \frac{\alpha\tilde{w}^2}{2} g = 0 \tag{IV.40}$$

A power series solution will solve Equation (IV.40) uniquely with initial conditions. But for the series to terminate, we must require $\alpha\tilde{w}^2/2$ to be equal to a nonnegative

even integer. With this requirement, the power series solution terminates into the well known Hermite polynomials:

$$g(\xi) = H_m(\xi) = H_m\left(\frac{\sqrt{2}\tilde{x}}{\tilde{w}}\right) \text{ where } m = 0, 1, 2, 3 \ldots \tag{IV.41}$$

There will be a similar solution for the $\tilde{y}$ terms of Equation (IV.31), i.e., $h(\eta) = H_n(\eta) = H_n(\sqrt{2}\tilde{y}/\tilde{w})$ where $n = 0, 1, 2, 3 \ldots$ The first ten Hermite polynomials are listed in Table II.

$H_0(x)$	=	1
$H_1(x)$	=	$2x$
$H_2(x)$	=	$4x^2 - 2$
$H_3(x)$	=	$8x^3 - 12x$
$H_4(x)$	=	$16x^4 - 48x^2 + 12$
$H_5(x)$	=	$32x^5 - 160x^3 + 120x$
$H_6(x)$	=	$64x^6 - 480x^4 + 720x^2 - 120$
$H_7(x)$	=	$128x^7 - 1344x^5 + 3360x^3 - 1680x$
$H_8(x)$	=	$256x^8 - 3584x^6 + 13440x^4 - 13440x^2 + 1680$
$H_9(x)$	=	$512x^9 - 9216x^7 + 48384x^5 - 80640x^3 + 30240x$

Table II. Hermite Polynomials from [12]

Returning to Equation (IV.31), we are left with finding a solution for $p(\tau)$. For Hermite solutions, α and β are constrained

$$\frac{\alpha\tilde{w}^2}{2} = 2m \rightarrow \alpha = \frac{4m}{\tilde{w}^2}$$
$$\frac{\beta\tilde{w}^2}{2} = 2n \rightarrow \beta = \frac{4n}{\tilde{w}^2}$$

Solving for $\overset{\circ}{p}$, with the constraints, and Equations (IV.34) and (IV.17),

$$-\frac{4}{\tilde{z}_o q} - 4i\overset{\circ}{p} = \alpha + \beta \tag{IV.42}$$

$$\begin{aligned} \overset{\circ}{p} &= \frac{i}{\tilde{w}^2}(m+n) + \frac{i}{\tilde{z}_o q} \\ &= i(m+n+1)\frac{\tilde{z}_o}{\tilde{z}_o^2 + \tau^2} + \frac{\tau}{\tilde{z}_o^2 + \tau^2} \end{aligned} \tag{IV.43}$$

Integrating and applying initial conditions for p

$$\begin{aligned} p(\tau) &= i(m+n+1)\tilde{z}_o \int_0^\tau \frac{\partial\tau'}{\tilde{z}_o^2+\tau'^2} + \int_0^\tau \frac{\tau'}{\tilde{z}_o^2+\tau'^2}d\tau' \\ &= i(m+n+1)\arctan\frac{\tau}{\tilde{z}_o} + \ln\sqrt{\frac{\tilde{z}_o^2+\tau^2}{\tilde{z}_o^2}} \end{aligned} \tag{IV.44}$$

So we now have all the pieces to Equation (IV.24). Putting it altogether, Equations (IV.34), (IV.41), and (IV.44) into (IV.24), and after a little tidying up, we arrive finally at an expression for the (m,n) mode for the laser optical field:

$$a_{m,n}(\tilde{\mathbf{r}},\tau) = \overbrace{a_o\frac{\tilde{w}_o}{\tilde{w}}H_m\left(\frac{\sqrt{2}\tilde{x}}{\tilde{w}}\right)H_n\left(\frac{\sqrt{2}\tilde{y}}{\tilde{w}}\right)e^{-\frac{\tilde{r}^2}{\tilde{w}^2}}}^{\text{Amplitude}}\underbrace{e^{i\phi_{m,n}(\tilde{\mathbf{r}},\tau)}}_{\text{Phase}} \tag{IV.45}$$

where the phase, $\phi_{m,n}$, is given by

$$\phi_{m,n}(\tilde{\mathbf{r}},\tau) = \frac{\tilde{r}^2\tau}{\tilde{w}_o^2\tilde{w}(\tau)^2} - (m+n+1)\arctan\frac{\tau}{\tilde{z}_o} \tag{IV.46}$$

Figure 19 shows the "burn patterns" for various modes.

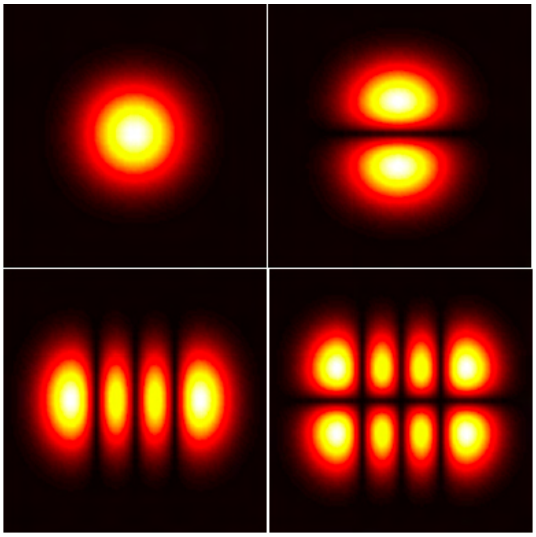

Figure 19. $|a_{00}|$, $|a_{01}|$, $|a_{30}|$, $|a_{31}|$ (Left to right; Top to bottom)

D. NORMALIZATION

If we attempt to superpose modes with high values of m or n, the Hermite polynomials with Gaussian envelopes for these higher modes have large coefficients as shown in Table II. To place all the modes on an equal footing we will normalize each of them to the power in the fundamental which is given by

$$P_{0,0} = \int_{-\infty}^{\infty}\int_{-\infty}^{\infty} |a_{0,0}|^2 d\tilde{x}d\tilde{y} \tag{IV.47}$$

Substituting Equation (IV.20) we have

$$P_{0,0} = a_o^2 \frac{\tilde{w}_o^2}{\tilde{w}^2}\int_{-\infty}^{\infty} e^{-\frac{2\tilde{x}^2}{\tilde{w}^2}} d\tilde{x}\int_{-\infty}^{\infty} e^{-\frac{2\tilde{y}^2}{\tilde{w}^2}} d\tilde{y} \tag{IV.48}$$

so then

$$P_{0,0} = \frac{\pi}{2} a_o^2 \tilde{w}_o^2 \tag{IV.49}$$

The power in an arbitrary mode is

$$P_{m,n} = \int_{-\infty}^{\infty}\int_{-\infty}^{\infty} |a_{m,n}|^2 d\tilde{x}d\tilde{y} \tag{IV.50}$$

Substituting Equation (IV.45) we have

$$P_{m,n} = \int_{-\infty}^{\infty}\int_{-\infty}^{\infty} a_o^2 \frac{\tilde{w}_o^2}{\tilde{w}^2} H_m^2 H_n^2 e^{-\frac{2\tilde{r}^2}{\tilde{w}^2}} d\tilde{x}d\tilde{y} \tag{IV.51}$$

To evaluate this integral, we make use of the fact that Hermite polynomials are orthogonal on the range$(-\infty,\infty)$ with respect to a weighting function [12],

$$\int_{-\infty}^{\infty} H_i(x)H_j(x)e^{-x^2}dx = \delta_{i,j}2^j j!\sqrt{\pi} \tag{IV.52}$$

where the $\delta_{i,j}$ is the Kronecker delta. To properly make use of the orthogonality condition, Equation (IV.52), we must first massage Equation (IV.51) into the correct form. Consider the factor

$$\int_{-\infty}^{\infty} H_m\left(\frac{\sqrt{2}\tilde{x}}{\tilde{w}}\right)^2 e^{-\frac{2\tilde{x}^2}{\tilde{w}^2}}\, d\tilde{x} \tag{IV.53}$$

If we make the following change of variables, let

$$\alpha = \frac{\sqrt{2}\tilde{x}}{\tilde{w}} \rightarrow \tilde{x} = \frac{\alpha\tilde{w}}{\sqrt{2}} \tag{IV.54}$$

so that,

$$d\tilde{x} = \frac{\tilde{w}}{\sqrt{2}}d\alpha \tag{IV.55}$$

Then Equation (IV.53) becomes

$$\frac{\tilde{w}}{\sqrt{2}}\int_{-\infty}^{\infty} H_m(\alpha)^2 e^{-\alpha^2} d\alpha \tag{IV.56}$$

Employing the orthogonality condition, Equation (IV.52) when $m' = m$, we have

$$\frac{\tilde{w}}{\sqrt{2}}\int_{-\infty}^{\infty} H_m(\alpha)^2 e^{-\alpha^2} d\alpha = \tilde{w}\sqrt{\frac{\pi}{2}}2^m m! \tag{IV.57}$$

and similarly for the $\tilde{y}$ factors. The power in the (m,n) mode then becomes

$$P_{m,n} = \frac{\pi}{2}a_o^2\tilde{w}_o^2 2^m 2^n m!n! \tag{IV.58}$$

$$= P_{0,0}2^m 2^n m!n! \tag{IV.59}$$

So the power in the (m,n) mode can be normalized to the power in the fundamental by dividing it through by $2^m 2^n m!n!$. A normalized expression for the optical field in the (m,n) mode is then

$$A_{m,n} = \frac{1}{\sqrt{2^m 2^n m!n!}}a_{m,n} \tag{IV.60}$$

This expression places all the higher-order modes on an equal footing; all modes have the same power as the fundamental.

E. FINDING COEFFICIENTS

The total optical field is a superposition of all the separate normalized components, i.e.,

$$A_T(\tilde{\mathbf{r}}, \tau) = \sum_{m,n}^{\infty} C_{m,n} A_{m,n}(\tilde{\mathbf{r}}, \tau) \tag{IV.61}$$

where $C_{m,n}$ is the normalized coefficient for the (m,n) mode. Each term, or component, is a solution to the wave equation. So, the sum of terms is also a solution.

Moreover, the Hermite-Gaussian modes form a complete orthogonal basis set [16] so that any laser field satisfying the wave equation can be accurately represented by Equation (IV.61) with appropriate coefficients $C_{m,n}$. Our task now is to determine the unknown normalized coefficients $C_{m,n}$. As with a Fourier series decomposition of a function, we can employ the Hermite analog of Fourier's Trick[2]. To determine the coefficients for an optical field, A_T, we multiply Equation (IV.61) by $A^*_{m',n'}$ and integrate over all $\tilde{x}$ and $\tilde{y}$ giving us

$$\int_{-\infty}^{\infty}\int_{-\infty}^{\infty} A_T \; A^*_{m',n'} \; d\tilde{x}d\tilde{y} = \int_{-\infty}^{\infty}\int_{-\infty}^{\infty} \sum_{m,n}^{\infty} C_{m,n} A_{m,n} \; A^*_{m',n'} \; d\tilde{x}d\tilde{y} \tag{IV.62}$$

where the asterisk denotes taking the complex conjugate. Expanding out the right hand side, we have

$$= \int_{-\infty}^{\infty}\int_{-\infty}^{\infty} \sum_{m,n}^{\infty} C_{m,n} \frac{1}{\sqrt{2^m 2^n m!n!}} a_o \frac{\tilde{w}_o}{\tilde{w}} H_m H_n e^{-\frac{\tilde{r}^2}{\tilde{w}^2}} e^{i\phi_{m,n}} \frac{1}{\sqrt{2^m 2^n m!n!}} a_o \frac{\tilde{w}_o}{\tilde{w}} H_{m'} H_{n'} e^{-i\phi_{m',n'}} \tag{IV.63}$$

Notice the term that involves the product of the phases from the unprimed and primed optical field. Recalling Equation (IV.46), we then have

$$\begin{aligned} e^{\phi_{m,n}} \; e^{-\phi_{m',n'}} &= e^{i(\phi_{m,n} - \; \phi_{m',n'})} \\ &= e^{i[((m' - \; m) \; + \; (n' - \; n)) \arctan \frac{\tau}{\tilde{z}_o}]} \end{aligned} \tag{IV.64}$$

This equation does not depend on $\tilde{x}$ or $\tilde{y}$, so we can pull it out of the integral. Returning to Equation (IV.63) and employing the orthogonality of Hermite polynomials when $m' = m$ and $n' = n$, we have

$$\int_{-\infty}^{\infty}\int_{-\infty}^{\infty} A_T \; A^*_{m,n} \; d\tilde{x}d\tilde{y} = C_{m,n} \frac{1}{2^m 2^n m!n!} \frac{a_o^2 \tilde{w}_o^2}{\tilde{w}^2} \left[\tilde{w}\sqrt{\frac{\pi}{2}} 2^m m!\right] \left[\tilde{w}\sqrt{\frac{\pi}{2}} 2^n n!\right] \tag{IV.65}$$

Combining this result with the left-hand side of Equation (IV.62), we have

$$C_{m,n} = \frac{2}{\pi a_o^2 \tilde{w}_o^2} \int_{-\infty}^{\infty}\int_{-\infty}^{\infty} A_T \; A^*_{m,n} \; d\tilde{x}d\tilde{y} \tag{IV.66}$$

---

[2][14], Chapter 3

This equation is an expression for the normalized coefficients for our optical field A_T. Our next task will be to write computer code to determine the coefficients of any waveform.

V. SIMULATIONS

In this chapter we will describe how numerical simulation can solve the non-linear differential equations that have been developed. Non-linear differential equations are exceedingly difficult to solve analytically but are relatively "easy" with a computer.

A. MODELING THE FREE ELECTRON LASER

In order to model the FEL we must simultaneously solve two coupled differential equations: the pendulum equation, Equation (III.32),

$$\overset{\circ\circ}{\zeta} = |a| \cos(\zeta + \phi)$$

and the FEL wave equation, Equation (III.64),

$$\left[-\frac{i}{4} \tilde{\boldsymbol{\nabla}}_{\perp}^{\mathbf{2}} + \frac{\partial}{\partial \tau} \right] a(\tilde{\mathbf{r}}, \tau) = < -j e^{-i\zeta} >$$

The pendulum equation updates electron phases and phase velocities and the wave equation propagates the light self-consistently with the electron beam interaction. The Naval Postgraduate School's Directed Energy and Electric Weapons Center uses an Apple Xserve cluster to model the FEL (see Figure 20). The cluster is specifically designed to model the FEL in four dimensions as well as model FEL performance due to perturbations or test validity of new designs.

In order to numerically solve Equation (III.64), fast Fourier transforms are used in the code [17]. An output for a recent simulation is given in Figure 21.

Figure 20. NPS Apple Xserve cluster with 64 nodes / 128 processors.

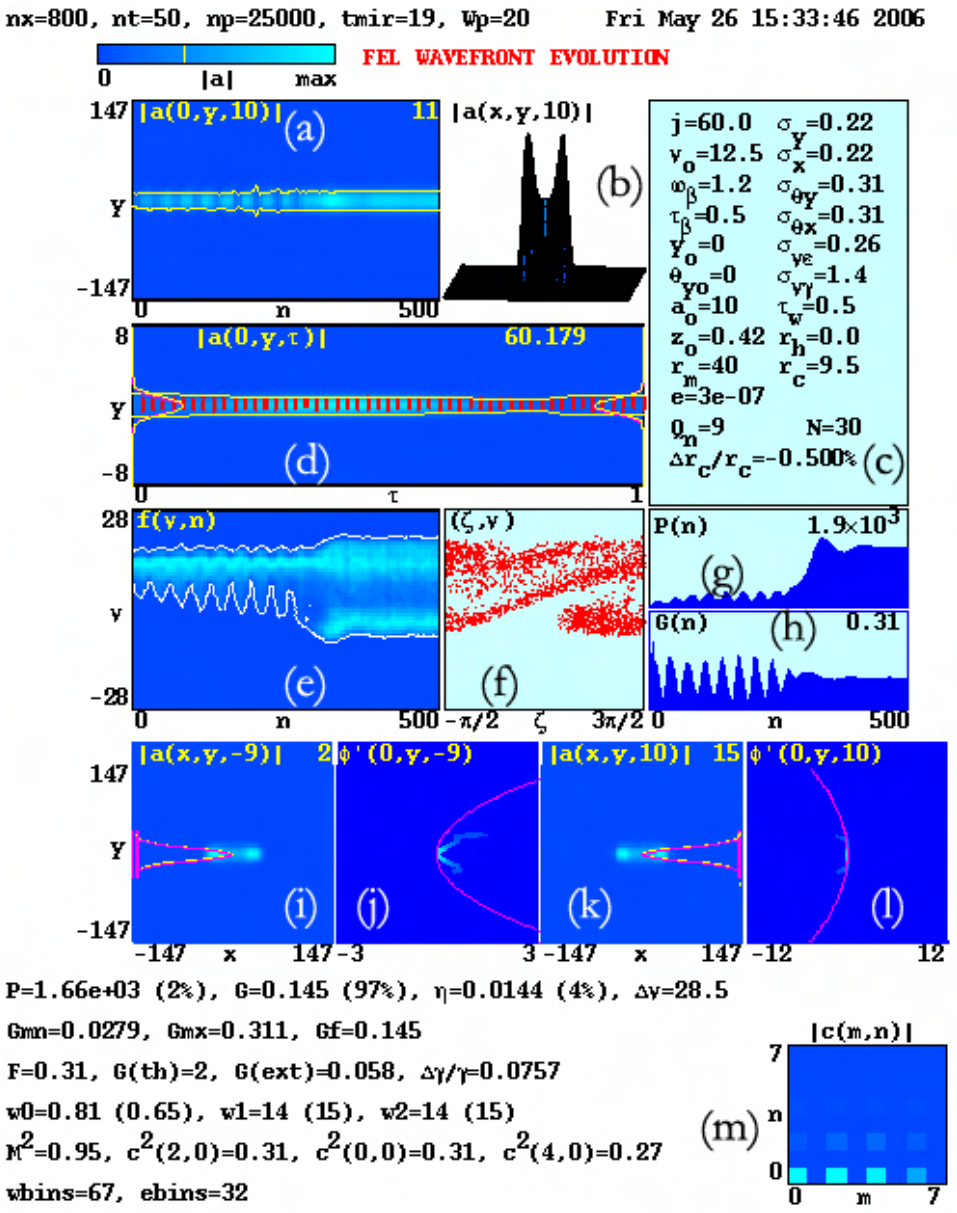

Figure 21. FEL simulation output. (a) Optical mode evolution over 500 passes at right mirror (b) Surface plot of the optical field at the right mirror after last pass; (c) User defined parameters (see Table (III)); (d) Cross section of optical mode and electron beam as it propagates from $\tau = 0 \rightarrow 1$ on last pass; (e) Evolution of electron beam distribution in phase velocity over 500 passes; (f) Electron phase space at $\tau = 1$ after last pass; (g) Optical power evolution over 500 passes; (h) Optical gain evolution over 500 passes; (i) Burn pattern of optical mode at left mirror after last pass; (j) Optical phase for at left mirror after last pass; (k) Burn pattern of optical mode at right mirror after last pass; (l) Optical phase for at right mirror for last pass; (m) Hermite-Gaussian coefficients for right mirror (Code is developed in this chapter)

Symbol	Name	Equation
j	Electron current density	$j = 8\pi^2 N e^2 K^2 L^2 \rho / \gamma^3 mc^2$
ν_o	Electron phase velocity	$\nu_o = [(k + k_o)\beta_z - k]L$
ω_β	Betatron frequency	$\omega_\beta = 2\pi NK/\gamma$
τ_β	Electron beam waist position	$\tau_\beta = Z_\beta / L$
y_o	Electron beam shift	$y_o = Y_o\sqrt{\pi/L\lambda}$
θ_{yo}	Electron beam tilt	$\theta_{yo} = \Theta\sqrt{L\pi/\lambda}$
a	Initial optical field amplitude	$\lvert a\rvert = 4\pi NeK\lvert E\rvert L/\gamma^2 mc^2$
z_o	Rayleigh length	$z_o = Z_o/L$
r_m	Dimensionless mirror radius	$r_m = R_m\sqrt{\pi/\lambda L}$
e	Mirror edge loss	See [18]
Q_n	Cavity quality factor	$Q_n = 1/$(loss per pass)
σ_x, σ_y	Electron beam radius	$\sigma_x = X_e\sqrt{\pi/L\lambda}$
$\sigma_{\theta x}$, $\sigma_{\theta y}$	Electron beam angular spread	
$\sigma_{\nu\epsilon}$	Spread in electron phase velocity due to emittance	See [18]
$\sigma_{\nu\gamma}$	Spread in electron phase velocity due to energy spread	See [18]
τ_w	Optical mode waist position	$\tau_w = Z_w/L$
r_h	Right mirror hole radius	$r_h = R_h\sqrt{\pi/\lambda L}$
r_c	Mirror radius of curvature	$r_c = R_c\sqrt{\pi/\lambda L}$

Table III. User-defined FEL simulation parameters

Each node of the Apple cluster can run a simulation such as the one shown above at a different values of ν_o simultaneously. We can then determine gain and extraction values at the optimum value of ν_o. This simulates what the FEL would do by mode competition.

The simulation also provides us with an array describing the optical field, $a(\tilde{x}, \tilde{y})$. As mentioned in the previous chapter, the optical field is a superposition of Hermite-Gaussian basis set with appropriately chosen coefficients. Mirror distortion or electron beam shifts and tilts can cause the optical field to develop higher-order modes. We will now analyze these modes by finding their coefficients numerically.

B. FINDING HERMITE-GAUSSIAN COEFFICIENTS NUMERICALLY

Equation (IV.66) is the analytical expression for the normalized Hermite-Gaussian (HG) coefficients. We need to recast this equation in a form that is computer-friendly. Since A_T and $A^*_{m,n}$ are complex, we can write:

$$A_T = A^r_T + iA^i_T \tag{V.1}$$

$$A^*_{m,n} = A^r_{m,n} - iA^i_{m,n} \tag{V.2}$$

where A^r_T and A^i_T are the real and imaginary parts of the total normalized optical field and $A^r_{m,n}$ and $A^i_{m,n}$ are the real and imaginary parts of the normalized (m,n) mode. Equation (IV.66) becomes

$$C_{m,n} = \frac{2}{\pi a_o^2 \tilde{w}_o^2} \int\int (A^r_T + iA^i_T)(A^r_{m,n} - iA^i_{m,n}) d\tilde{x}\ d\tilde{y} \tag{V.3}$$

Expanding out the factors and separating the coefficients into their real and imaginary parts, we have

$$C^r_{m,n} = \frac{2}{\pi a_o^2 \tilde{w}_o^2} \int\int (A^r_T\, A^r_{m,n} + A^i_T\, A^i_{m,n})\, d\tilde{x}\ d\tilde{y} \tag{V.4}$$

$$C^i_{m,n} = \frac{2}{\pi a_o^2 \tilde{w}_o^2} \int\int (A^i_T\, A^r_{m,n} - A^r_T\, A^i_{m,n})\, d\tilde{x}\ d\tilde{y} \tag{V.5}$$

and

$$|C_{m,n}|^2 = (C^r_{m,n})^2 + (C^i_{m,n})^2 \tag{V.6}$$

So, let us first describe the procedure for developing a numerical modal analysis tool in the C programming language:

1. Construct Hermite-Gaussian basis arrays.
2. Read in or form a user-defined optical field.
3. Determine HG coefficients via Equations (V.4), (V.5), and (V.6)

Our expression for the optical field, Equation (IV.61) is a sum of the normalized basis at some time τ. Recall that the optical field is a complex number so we must keep track of the real and imaginary parts. These analytical expressions are continuous in $\tilde{x}$ and $\tilde{y}$ so we recast the expression for the (m,n) mode into their real and imaginary parts over the discrete sites in the array. Therefore, in pseudo-code we have

$$A^r[m][n][\tilde{x}_j][\tilde{y}_k] =$$

$$a_o \frac{\tilde{w}_o}{\tilde{w}} H_m\left(\frac{\sqrt{2}\tilde{x}_j}{\tilde{w}}\right) H_n\left(\frac{\sqrt{2}\tilde{y}_k}{\tilde{w}}\right) e^{-\frac{\tilde{r}_{j,k}^2}{\tilde{w}^2}} \cos\left(\frac{\tilde{r}_{j,k}^2 \tau}{\tilde{w}_o^2 \tilde{w}^2} - (m+n+1)\arctan\frac{\tau}{\tilde{z}_o}\right) \quad \text{(V.7)}$$

$$A^i[m][n][\tilde{x}_j][\tilde{y}_k] =$$

$$a_o \frac{\tilde{w}_o}{\tilde{w}} H_m\left(\frac{\sqrt{2}\tilde{x}_j}{\tilde{w}}\right) H_n\left(\frac{\sqrt{2}\tilde{y}_k}{\tilde{w}}\right) e^{-\frac{\tilde{r}_{j,k}^2}{\tilde{w}^2}} \sin\left(\frac{\tilde{r}_{j,k}^2 \tau}{\tilde{w}_o^2 \tilde{w}^2} - (m+n+1)\arctan\frac{\tau}{\tilde{z}_o}\right) \quad \text{(V.8)}$$

where A^i and A^r are four-dimensional arrays indexed by the mode number and position, given by (m,n) and ($\tilde{x}_j$, $\tilde{y}_k$), respectively. We calculate the basis set for the first several modes and store these values in their arrays. We then read in the optical field that is passed as an array from the main FEL simulation or form a user-defined field[1] by a linear combination of normalized Hermite-Gaussian modes using the arrays that been calculated.

We determine the HG coefficients via Equations (V.4), (V.5), and (V.6). We approximate the double integral by nested loops over m, n, and over the number of array sites, nx. In pseudo-code,

$$C^r[m][n] = \frac{2}{\pi a_o^2 \tilde{w}_o^2} \sum_k^{nx} \sum_j^{nx} \left(A_T^r[\tilde{x}_j][\tilde{y}_k]\, A^r[m][n][\tilde{x}_j][\tilde{y}_k] + A_T^i[\tilde{x}_j][\tilde{y}_k]\, A^i[m][n][\tilde{x}_j][\tilde{y}_k]\right) \quad \text{(V.9)}$$

and

$$C^i[m][n] = \frac{2}{\pi a_o^2 \tilde{w}_o^2} \sum_k^{nx} \sum_j^{nx} \left(A_T^i[\tilde{x}_j][\tilde{y}_k]\, A^r[m][n][\tilde{x}_j][\tilde{y}_k] - A_T^r[\tilde{x}_j][\tilde{y}_k]\, A^i[m][n][\tilde{x}_j][\tilde{y}_k]\right) \quad \text{(V.10)}$$

[1]A user-defined field can be used as a check on the code to ensure that it is operating properly.

The square of the magnitude of the HG coefficient for the (m,n) mode is then given by Equation (V.6), that is,

$$C[m][n]^2 = (C^r[m][n])^2 + (C^i[m][n])^2 \tag{V.11}$$

It is convenient to normalize the square of the magnitudes to the power of the total field A_T. The power in the total field is given by

$$P_T = \int_{-\infty}^{\infty}\int_{-\infty}^{\infty} |A_T|^2 d\tilde{x}d\tilde{y} \tag{V.12}$$

Substituting Equation (IV.61) and working out the integrals we find that

$$P_T = \frac{\pi}{2} a_o^2 \tilde{w}_o^2 \sum_{m,n}^{\infty} C_{m,n}^2 \tag{V.13}$$

Recall that the power in the fundamental mode is given by $P_{0,0} = \pi a_o^2 \tilde{w}_o^2/2$ so that the total power in the optical field is then (in terms of the fundamental)

$$P_T = P_{0,0} \sum_{m,n}^{\infty} C_{m,n}^2 \tag{V.14}$$

The fractional power spectrum, $S[m][n]$, is then

$$\mathrm{S[m][n]} = \frac{C[m][n]^2}{\sum_{i,j} C[i][j]^2} \tag{V.15}$$

where $\sum_{i,j} C[i][j]^2$ is the sum of all the squares of the normalized mode coefficients.

To illustrate how the code works, consider the following examples illustrated in Figures 22 and 23. In Figure 22 (a), the diagnostic correctly identifies the fractional power spectrum as 50% in both $A_{0,2}$ and $A_{2,0}$ modes. Incidentally, the superposition of equally weighted $A_{0,2}$ and $A_{2,0}$, with no relative phase difference between them, results in a pure L_1^0 Laguerre-Gaussian mode[2].

In Figure 22 (b), the diagnostic correctly identifies the fractional power spectrum for the superposition of $A_{0,0}$, $A_{1,1}$, and $A_{3,3}$ with $C_{0,0} = 1$, $C_{1,1} = 2$, and $C_{3,3} = 3$

[2]To see this: ask Professor Colson and he will buy you a beer.

as 7%, 28%, and 64%, respectively. A screen capture of Cmn.c is shown in Figure 23 for this case. As you can see, the program outputs the Rayleigh length and mode waist. It then displays the mode radius at $\tau = 0$, the power in the fundamental, and total power in the arbitrary field. The fractional power spectrum is then calculated and displayed. The code then propagates the optical field in free-space and performs the same analysis on the final waveform.

In Figure 22 (c), the diagnostic correctly identifies the fractional power spectrum for the superposition of equally weighted $A_{0,0}$, $A_{0,2}$, and $A_{0,4}$ modes. We will see a similar combinations of even 'm' and 'n' valued modes when we investigate mirror distortions.

The diagnostic developed for this thesis for Hermite-Gaussian modal analysis was then incorporated into the main NPS FEL simulation code as a function call. In the next chapter, we will see this diagnostic in action when we simulate mirror distortions.

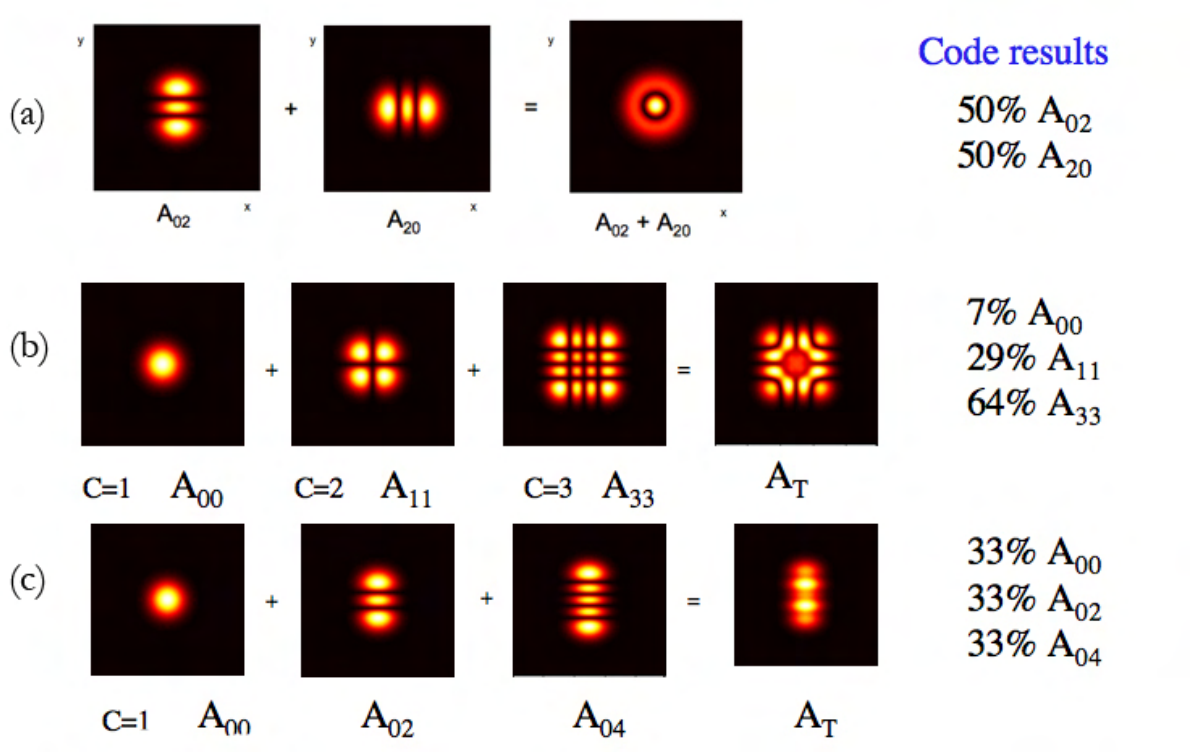

Figure 22. Graphics from Cmn.c output was drawn with MatLab (a) Superposition of equally weighted $A_{0,2}$ and $A_{2,0}$. (b) Superposition of $A_{0,0}$, $A_{1,1}$, and $A_{3,3}$ with $C_{0,0} = 1$, $C_{1,1} = 2$, and $C_{3,3} = 3$. (c) Superposition of equally weighted $A_{0,0}$, $A_{0,2}$, and $A_{0,4}$.

```
Files opened
Initializations
zo = 0.5          tauw = 0.5

Loading up basis sets at tau = 0.

w(0) = 1
P_00(tau = 0) = 78.5398
P_T(0) = 1099.56
Outputting initial wavefront to file

Calculating initial Cmns

Normalized initial cmn amplitudes squared
Cmn2[0][0] = 0.0714286
Cmn2[1][1] = 0.285714
Cmn2[3][3] = 0.642857

Propagating waveform...

w(1) = 1
P_00(1) = 78.5398
P_T(1) = 1119.46

Normalized initial cmn amplitudes squared
Cmn2[0][0] = 0.0702047
Cmn2[1][1] = 0.28182
Cmn2[3][3] = 0.639894


Closing files...
span105-250:~/Desktop/Current Code rvigilpbg4$
```

Figure 23. Output from diagnostic tool Cmn.c

VI. MIRROR DISTORTIONS

A. COLD CAVITY THEORY

In the pursuit of a weapons class FEL, high power and high intensity can lead to mirror distortions if heat deposited by the laser light to the mirror substrate isn't removed by cooling in a uniform manner. Distortions then cause higher-order modes to appear. It is important to quantify the fractional power spectrum among the higher-order modes because doing so uniquely identifies the laser field and may allow for corrective optics to single out the best modes for FEL lethality. We will investigate three different cases of mirror distortions on the outcoupling mirror: hyperbolic, ellipsoidal, and spherical. Hyperbolic and ellipsoidal distortions can be classified as a mirror astigmatism. It occurs when the radius of curvature of the spherical mirror along an axis differs by some small amount when compared to the perpendicular axis. For simplicity we chose these axes to line up with $\tilde{x}$ and $\tilde{y}$. Spherical distortion is not astigmatism because both axis are changed in exactly the same amount and in the same direction. Spherical distortions do change the Rayleigh length. Before we consider the effects of mirror distortions on FEL operation, let us explore cold-cavity effects (i.e., no electron beam present) of mirror "errors" to get a flavor for how the FEL might respond. Keep in mind that cold-cavity theory discussed in this section keeps both mirrors the same. The dimensionless radius of curvature of the two ideal mirrors determines the Rayleigh length, $\tilde{z}_o$ [18], and is given by[1]

$$\tilde{r}_c = \frac{\tau_m}{2} + \frac{2\tilde{z}_o^2}{\tau_m} \tag{VI.1}$$

where τ_m is the dimensionless mirror separation. Factoring out $\tau_m/2$ and defining a small parameter $\kappa = 4\tilde{z}_o^2/\tau_m^2$, we then have

$$\tilde{r}_c = \frac{\tau_m}{2}(1+\kappa) \tag{VI.2}$$

[1]Symmetric confocal cavity. See [19], chapter 12.

where $\kappa << 1$ for $\tau_m >> \tilde{z}_o$. Typically, $\tau_m \approx 10$ and $\tilde{z}_o \approx 0.1$, so $\kappa \approx 4$ x 10^{-4}. What if an actual mirror differs from the ideal mirror by a small amount? This could occur because mirror heating has distorted both mirrors, for instance. We can quantify this distortion as follows

$$\tilde{r}_c \rightarrow \tilde{r}_c(1+\epsilon) \tag{VI.3}$$

where ϵ is a small deviation from the original radius of curvature $\tilde{r}_c$. Combining these relations we have

$$\tilde{r}_c = \frac{\tau_m}{2}(1+\kappa)(1+\epsilon) \tag{VI.4}$$

$$\tilde{r}_c = \frac{\tau_m}{2}(1+\kappa+\epsilon+\kappa\epsilon) \tag{VI.5}$$

Since κ and ϵ are small, we can approximate this equation to first order giving us

$$\tilde{r}_c \approx \frac{\tau_m}{2}(1+\kappa+\epsilon) \tag{VI.6}$$

We now ask, "What is going on with the mode radius at the waist and at the outcoupling mirror with respect to κ and τ_m?" The waist is given by

$$\tilde{w}_o = \sqrt{\tilde{z}_o} \tag{VI.7}$$

We can solve Equation (VI.1) for $\tilde{z}_o$ giving us

$$\tilde{z}_o = \frac{\tau_m}{2}\left(\frac{2\tilde{r}_c}{\tau_m} - 1\right)^{\frac{1}{2}} \tag{VI.8}$$

and substitute that into our expression for the waist giving us

$$\tilde{w}_o = \left(\frac{\tau_m}{2}\right)^{\frac{1}{2}}\left(\frac{2\tilde{r}_c}{\tau_m} - 1\right)^{\frac{1}{4}} \tag{VI.9}$$

Substituting Equation (VI.6), we now have

$$\tilde{w}_o \approx \left(\frac{\tau_m}{2}\right)^{\frac{1}{2}}\left(\frac{2}{\tau_m}\frac{\tau_m}{2}(1+\kappa+\epsilon) - 1\right) \tag{VI.10}$$

$$\tilde{w}_o \approx \left(\frac{\tau_m}{2}\right)^{\frac{1}{2}}(\kappa+\epsilon)^{\frac{1}{4}} \tag{VI.11}$$

Let us now consider the mode radius at the mirror. The mode radius is given by Equation (IV.17). At the outcoupling mirror, $\tau = \tau_m/2$, we then have

$$\tilde{w}(\tau_m/2) = \tilde{w}_m = \sqrt{\tilde{z}_o + \frac{\tau_m^2}{4\tilde{z}_o}} \tag{VI.12}$$

Substituting Equations (VI.6) and (VI.8) in for $\tilde{z}_o$ and after a little algebra we arrive at

$$\tilde{w}_m = \sqrt{\frac{\tilde{z}_o}{\kappa + \epsilon}} \tag{VI.13}$$

In both Equations (VI.11) and (VI.13), there is a problem when the mirror distortion $\epsilon \to -\kappa$. Let us plot these two equations with respect to ϵ/κ. From Figure 24 we

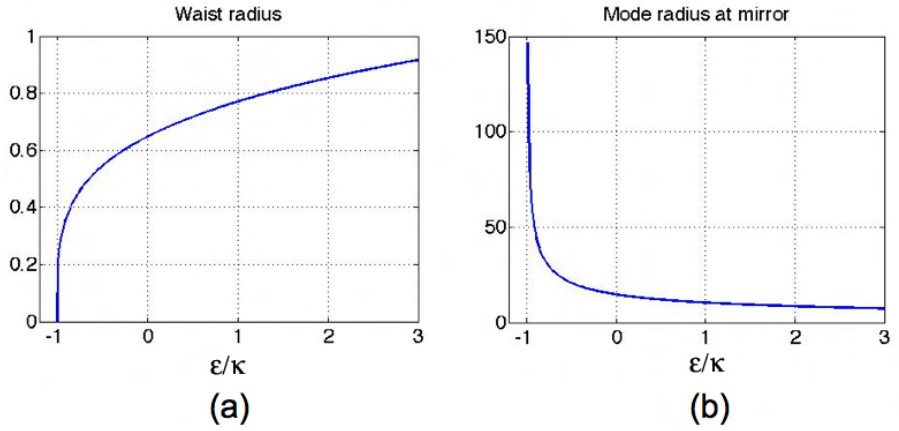

Figure 24. Cold-cavity. (a) Waist radius variation (b) Mode radius variation at the outcoupling mirror.

can see that if the error, ϵ is less than $-\kappa$ the waist radius and mode radius becomes imaginary. If $\epsilon = -\kappa$, the waist radius becomes zero and the mode radius at the mirror becomes infinity. So, as far as cold-cavity analysis predicts, mode radius can be sensitive to mirror distortions that are on the order of $-\kappa$. So we may expect actual FEL operation to follow a similar trend.

We chose to simulate the effects of mirror distortions on two different JLab oscillator configurations: Electromagnetic (EM) wiggler and STI Optronics wiggler designs. The following table highlights their major differences.

	EM wiggler	STI wiggler
Undulator period, λ_o (cm)	8	5.5
Undulator parameter, K	0.5	1.36
Undulator length, L (m)	2.3	1.65
No. Periods, N	29	30
Mirror Separation, S (m)	30	50
Quality factor, Q_n	25	9
Rayleigh length, Z_o (cm)	90	70
κ (%)	0.35	0.2

Table IV. JLab EM and STI wiggler comparison

B. HYPERBOLIC DISTORTION

In the case of hyperbolic distortion, we vary the mirror distortion on the outcoupling mirror in the following way:

$$\Delta\tilde{r}_{c\tilde{y}} = -\Delta\tilde{r}_{c\tilde{x}} \tag{VI.14}$$

where $\Delta\tilde{r}_{c\tilde{y}}$ and $\Delta\tilde{r}_{c\tilde{x}}$ are the changes of outcoupling mirror radius-of-curvature in the $\tilde{x}$ and $\tilde{y}$ directions, respectively. First let us consider the EM wiggler design. The results for gain and extraction are shown in Figure 25. Notice how both the gain and extraction graphs are symmetric about zero ϵ as should be expected for a hyperbolic distortion. Although, cold cavity analysis predicts catastraphic results when mirror distortions are less than $-\kappa$, we see that with FEL operation both the gain and extraction curves continues well beyond this cold cavity limit ($-\kappa$ is indicated by the red tick mark).

Notice also a peak in gain and extraction as the magnitude of ϵ is increased. It seems counterintuitive that increasing hyperbolic mirror distortion would improve

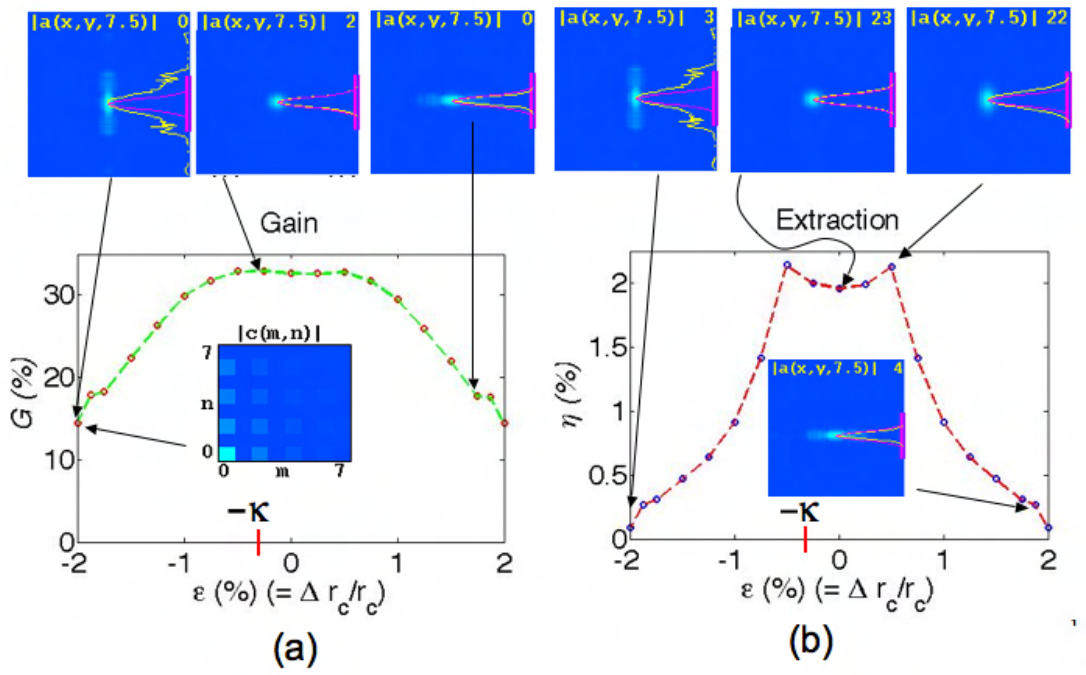

Figure 25. (a) Gain trend for hyperbolic distortion for the JLab EM wiggler. (b) Extraction trend for hyperbolic distortion for the JLab EM wiggler

FEL operation. This can be explained if we look at at Figure 25 (b). If we compare the burn patterns for $\epsilon = 0$ and $\epsilon = 0.5\%$, we can see that the mode shape at the mirror (yellow) is wider for the $\epsilon = 0.5\%$ case than for the $\epsilon = 0\%$ case. If the mode is more spread out at the mirror, we can conclude that the mode was more tightly focused in the undulator leading to a greater interaction between the optical mode and the electron beam leading to greater gain and extraction. This beneficial effect does not go on indefinitely. Eventually greater distortion will cause the mode to become so large that the mode will be clipped by the outcoupling mirror reducing gain and extraction. An example of a mode being clipped is shown in Figure 25 (a) for the $\epsilon = -2\%$ case. We also show the modal coefficients that comprise this data point. Notice that the 'n' modes are weighted more heavily than the 'm' modes since the burn pattern is spread out in the $\tilde{y}$ direction and that only even modes are present

since the original wave shape is assumed to be a fundamental Gaussian. Only the even modes overlap the origin ($\tilde{x} = 0, \tilde{y} = 0$) where the electron beam is amplifying the light.

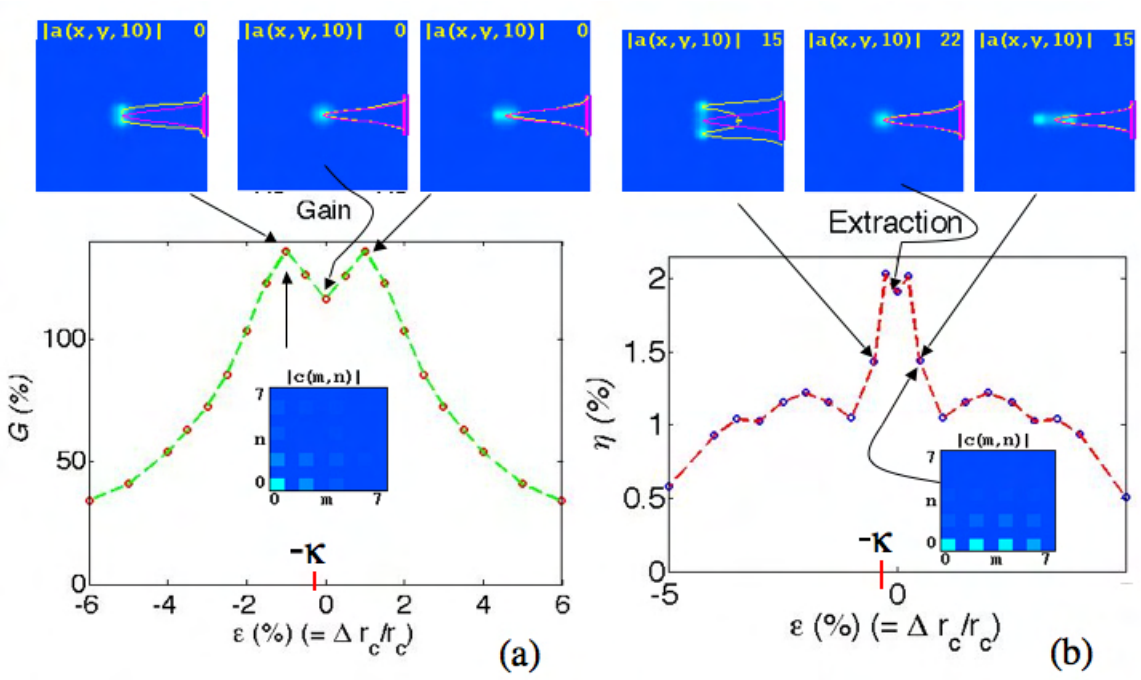

Figure 26. (a) Gain trend for hyperbolic distortion for the JLab STI wiggler. (b) Extraction trend for hyperbolic distortion for the JLab STI wiggler

We next considered the STI wiggler design. The results for gain and extraction are shown in Figure 26. As with the EM wiggler case, we see that the gain and the extraction are symmetric. The gain is much larger in the STI wiggler design due to a larger value of the undulator parameter, K. The mirror separation is greater, thereby yielding a somewhat smaller value for κ ($\kappa_{EM} = 0.35\%$ vs. $\kappa_{STI} = 0.2\%$). We also see a rise in gain and extraction for distortions on the order of $|\kappa|$ as in the EM wiggler case. Notice in Figure 26 (b) for $\epsilon = 0.5\%$, how the coefficients are strongly weighted in the 'm' modes due to a spreading out in the $\tilde{x}$ direction. Again, only the even modes are driven by the electron beam at the origin.

C. ELLIPSOIDAL DISTORTION

In ellipsoidal distortion, we vary the mirror error on the outcoupling mirror in the following way:

$$\text{vary } \Delta\tilde{r}_{c\tilde{y}} \ , \ \Delta\tilde{r}_{c\tilde{x}} = 0 \tag{VI.15}$$

As before, let us consider the EM wiggler results. Notice in Figure 27, both the gain

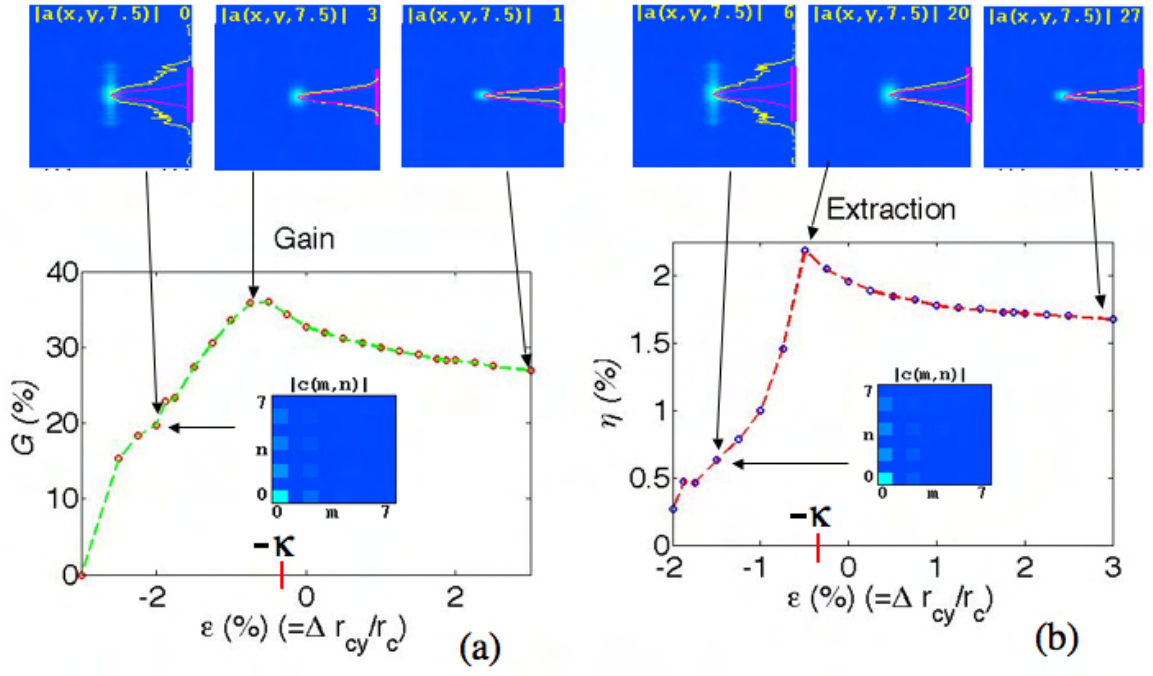

Figure 27. (a) Gain trend for ellipsoidal distortion for the JLab EM wiggler. (b) Extraction trend for ellipsoidal distortion for the JLab EM wiggler

and extraction curves are not symmetric, as should be expected for an asymmetric distortion. Both gain and extraction curves have the same general shape as Figure 24 (a). Unlike the cold cavity case, the FEL operates well beyond $\epsilon < -\kappa$. As ϵ is decreased further, higher-order modes appear as shown in the coefficient chart. Conversely, as ϵ is increased ($\epsilon > -\kappa$), the mode remains near the fundamental mode.

In Figure 28, we have the results for ellipsoidal distortions in the STI wiggler. Both curves are once again asymmetric. Notice how the gain curve reaches its max-

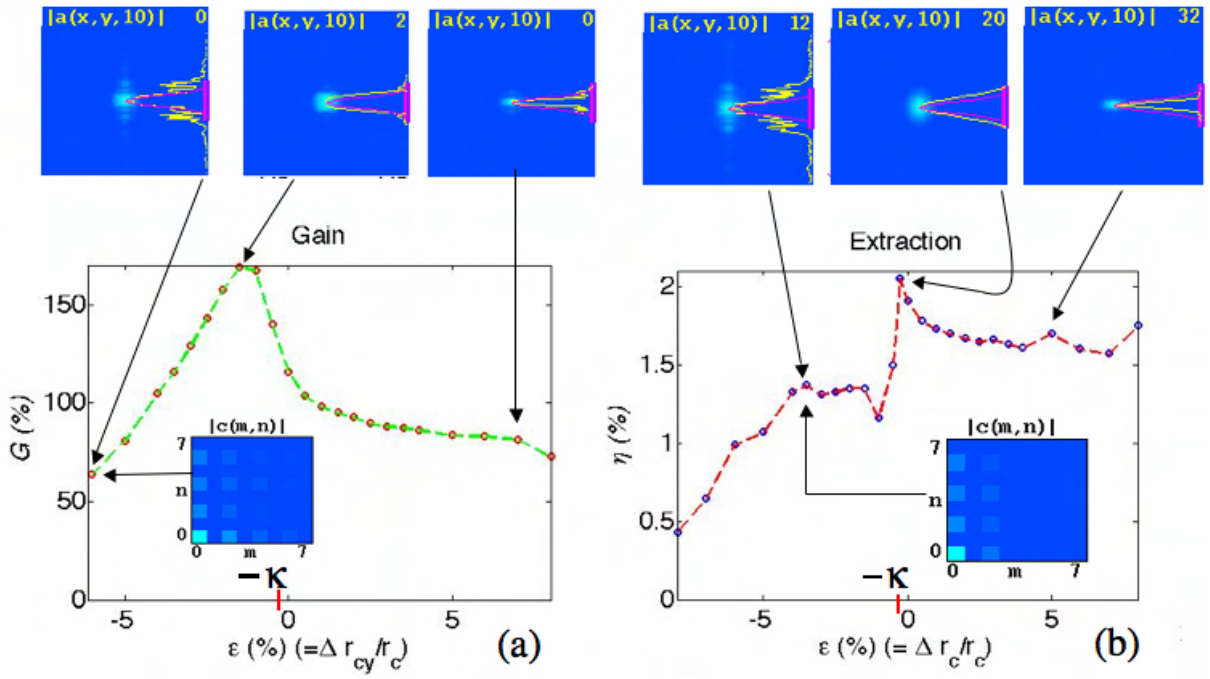

Figure 28. (a) Gain trend for ellipsoidal distortion for the JLab STI wiggler. (b) Extraction trend for ellipsoidal distortion for the JLab STI wiggler

imum at $\epsilon = -1.5\%$ which is several times greater than cold-cavity theory predicts the resonator should fail. The extraction curve is not as smooth as the EM wiggler extraction curve. But the general shape is still present, i.e., maximum nigh $-\epsilon$ and a relatively flat extraction in the positive ϵ direction.

D. SPHERICAL DISTORTION

In spherical distortion, we vary the mirror distortion on the outcoupling mirror in the following way:

$$\text{vary} \quad \Delta\tilde{r}_{c\tilde{y}} = \Delta\tilde{r}_{c\tilde{x}} \tag{VI.16}$$

Spherical distortion is not a misnomer even though the mirror remains cylindrically symmetric, because the highly reflecting mirror is not altered. The high power laser beam is assumed to have caused a symmetric distortion, as in Equation (VI.16). Res-

onator cavity instabilities are introduced as the distortion is increased or decreased. Notice in Figure 29, the burn patterns are cylindrically symmetric. Again, we see

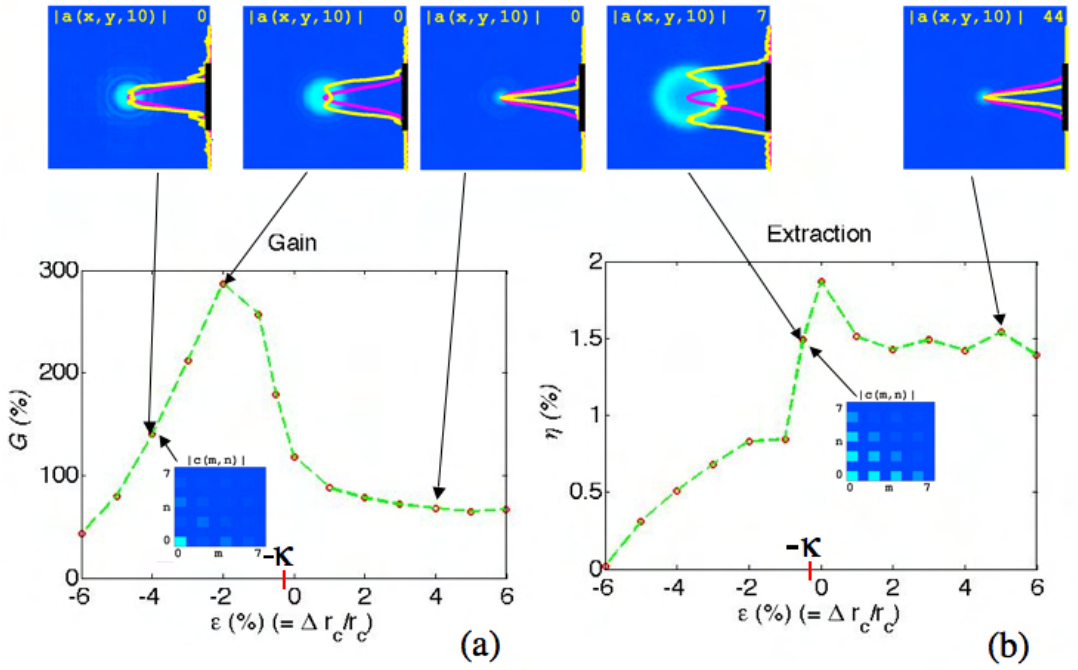

Figure 29. (a) Gain trend for spherical distortion for the JLab STI wiggler. (b) Extraction trend for spherical distortion for the JLab STI wiggler

good gain and extraction well into the regime where cold-cavity theory predicts a non-functioning FEL. Modal decomposition reveals an equal weighting of lower-order modes yielding burn patterns with central holes in them. Spherical distortion varies the effective cavity Rayleigh length. In Figure 30, we notice the burn patterns caused by varying Rayleigh length are cylindrically symmetric and comprised of equally weighted modes similar to spherical distortions. In Figure 30 (a), gain increases as we go to shorter Rayleigh lengths because the mode is more focused in the interaction region (see Figure 14) increasing the value of the filling factor. Since, gain is proportional to the filling factor, gain goes up. Shorter Rayleigh lengths expands the mode on the mirrors. In Figure 30 (b), the green curve shows a decreasing intensity

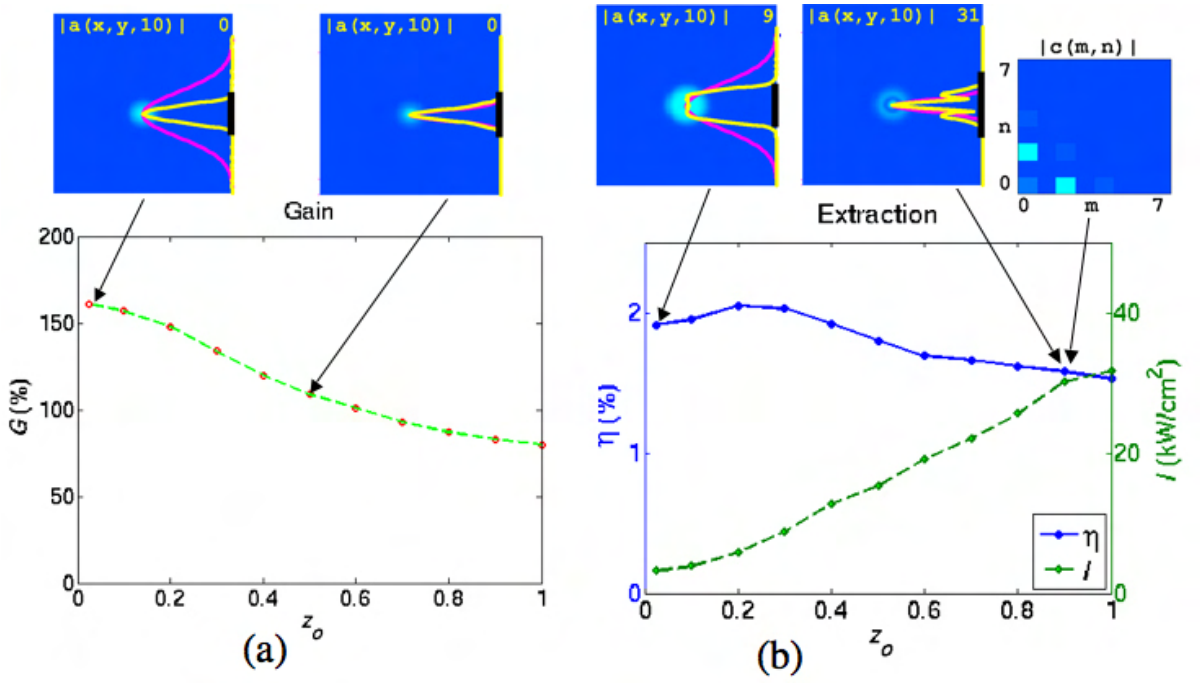

Figure 30. (a) Gain trend for Rayleigh length variation in the JLab STI wiggler. (b) Extraction and mirror intensity trends for Rayleigh length variation in the JLab STI wiggler

with decreasing Rayleigh length. This is good for FEL optics because the decreased intensity will mitigate mirror distortions caused by uneven heating or cooling.

VII. CONCLUSION

In this thesis, we have reviewed free electron laser theory and for the first time developed analytical solutions to quantify Hermite-Gaussian higher-order modes, developed a diagnostic for modal analysis, and investigated tolerance limits on mirror distortions. Hermite-Gaussian modes form a complete and orthogonal basis set that can fully describe any optical field and is a natural basis set when describing mirror distortions that do not possess cylindrical symmetry.

Modal analysis is a useful tool for describing mode quality. We are able to identify the fractional power spectrum in higher-order modes. This information may be used by an adaptive optics system to single out the best modes for propagation and lethality.

Tolerance limits on mirror distortions are several times greater than what cold cavity theory predicts. This is due to the electron beam not allowing the optical mode to shrink to zero size. The electron beam stabilizes the operation of the FEL. Simulations indicate JLab FEL should tolerate mirror distortions several percent, which is much greater than cold-cavity predictions. Finally, we recommend the following future work:

- Investigate Laguerre-Gaussian modes as another complete and orthogonal basis set to include azimuthal dependence.
- Incorporate both Hermite-Gaussian and Laguerre-Gaussian modal decomposition in the complete four dimensional FEL simulation program.
- Utilizing the diagnostic tool, investigate higher-order modes that appear due to mirror shifts/tilts and electron beam shifts/tilts.
- Choose a catchy and snappy name for NPS FEL simulation software....something other than wavens.

THIS PAGE INTENTIONALLY LEFT BLANK

APPENDIX A. CODES

We present the following programs used for finding Hermite-Gaussian coefficients of an arbitrary optical field and the MatLab scripts used in plotting. Line numbers are included for convenience.

1. CMN.C

```
/ * start of Cmn.c */
     1 // LCDR Ricardo Vigil
     2 // Thesis work
     3 // June 2006 graduation date
     4 // 13 major revisions
     5
     6 /* Program functions:
     7 - Combines up to ten user defined Hermite Gaussian modes
     8   to form an initial optical field
     9 - Decomposes the initial optical field into its constituent HG modes
    10 - Propagates the waveform in free space
    11 - Decomposes the propagated waveform into its constituent HG modes.
    12
    13 input files: Cmn.in
    14
    15 output files:
    16 initial.out - (x,y) initial amplitude in optical field, i.e, at tau = 0
    17 final.out - (x,y) final amplitude in optical field, i.e., at tau = 1
    18 ytau.out    - (y,t) amplitude cross section in (y, tau = 0 to 1)
    19
    20 Matlab graphics file: Coeffs.m
    21 Creates 5 graphics
    22 1. Amplitude burn pattern at tau = 0
    23 2. Amplitude surface plot at tau = 0
    24 3. Amplitude burn pattern at tau = 1
    25 4. Amplitude surface plot at tau = 1
    26 5. Propagation cross section in y vs tau
    27
    28 */
    29
    30 #include <stdio.h>
    31 #include <stdlib.h>
```

```
32 #include <math.h>
33
34
35 /* these arrays are defined outside main() due to segmentation faults */
36
37 double Abinitialr[10][10][200][200]; // real: (m,n) tau = 0
38 double Abinitiali[10][10][200][200]; // img:  (m,n) tau = 0
39 double Abfinalr[10][10][200][200];   // real: (m,n) tau = 1
40 double Abfinali[10][10][200][200];   // img: (m,n) tau = 1
41
42 int main(){
43
44  double P0=0.0, P1=0.0, rsq=0.0, dx=0.0, dy=0.0, C=0.0, wi=0.0, wf=0.0;
45  double Ao=0.0, zo=0.0, wo=0.0, tau=0.0, tauw=0.0, dtau=0.0, phi=0.0;
46  double c2sumInitial=0.0, c2sumFinal=0.0, temp1=0.0, temp2=0.0;
47  double Hx=0.0, Hy=0.0, ampinitial=0.0, ampfinal=0.0, ampy=0.0, K=0.0;
48  double pi=3.1415926, u=0.0, v=0.0;
49
50  double cinitialr[10][10];   // real: inital coeff for the mth nth mode
51  double cinitiali[10][10];   // img: intial coeff for the mth nth mode
52  double c2maginitial[10][10];// initial magnitude squared for (m,n) mode
53  double cfinalr[10][10];     // real: final coeff for the mth nth mode
54  double cfinali[10][10];     // img: final coeff for the mth nth mode
55  double c2magfinal[10][10];  // final magnitude squared for (m,n) mode
56  double iS[10][10];  // initial power spectrum ratio for (m,n) mode
57  double fS[10][10];  // final power spectrum ratio for (m,n) mode
58
59  double Powerinitial[10][10]; //Power in (m,n) normalized.
60  double Powerfinal[10][10];   //Power in (m,n) normalized.
61
62  double Atr[200][200];     //real: total real optical field
63  double Ati[200][200];     //img: total img optical field
64  double Atr_old[200][200]; //old values: real
65  double Ati_old[200][200]; //old values: img
66
67  int i=0,j=0,k=0,l=0,nx=0,W=0,x=0,y=0;
68  double c0=0.0,c1=0.0,c2=0.0,c3=0.0,c4=0.0;
69  double c5=0.0,c6=0.0,c7=0.0,c8=0.0,c9=0.0;
70  int m0=0,m1=0,m2=0,m3=0,m4=0,m5=0,m6=0,m7=0,m8=0,m9=0;
71  int n0=0,n1=0,n2=0,n3=0,n4=0,n5=0,n6=0,n7=0,n8=0,n9=0,count1=0;
72  unsigned int f;
73  unsigned int factorial(unsigned int a);
```

```
 74
 75  int m[10], n[10];
 76  double c[10];
 77
 78  FILE *input, *initial, *final, *ytau;
 79  input = fopen("Cmn.in","r");
 80  initial = fopen("initial.out","w");
 81  final = fopen("final.out","w");
 82  ytau = fopen("ytau.out","w");
 83
 84  printf("Files opened\n");
 85
 86  fscanf(input,"%lf %d %d",&c0,&m0,&n0);
 87  fscanf(input,"%lf %d %d",&c1,&m1,&n1);
 88  fscanf(input,"%lf %d %d",&c2,&m2,&n2);
 89  fscanf(input,"%lf %d %d",&c3,&m3,&n3);
 90  fscanf(input,"%lf %d %d",&c4,&m4,&n4);
 91  fscanf(input,"%lf %d %d",&c5,&m5,&n5);
 92  fscanf(input,"%lf %d %d",&c6,&m6,&n6);
 93  fscanf(input,"%lf %d %d",&c7,&m7,&n7);
 94  fscanf(input,"%lf %d %d",&c8,&m8,&n8);
 95  fscanf(input,"%lf %d %d",&c9,&m9,&n9);
 96  fscanf(input,"%lf %d %d",&Ao,&W,&nx);
 97  fscanf(input,"%lf %lf %lf",&zo,&tauw,&dtau);
 98
 99 /* initializations------------------------------ */
100
101  printf("Initializations\n");
102
103  c[0]=c0; c[1]=c1; c[2]=c2; c[3]=c3; c[4]=c4;
104  c[5]=c5; c[6]=c6; c[7]=c7; c[8]=c8; c[9]=c9;
105
106  m[0]=m0; m[1]=m1; m[2]=m2; m[3]=m3; m[4]=m4;
107  m[5]=m5; m[6]=m6; m[7]=m7; m[8]=m8; m[9]=m9;
108
109  n[0]=n0; n[1]=n1; n[2]=n2; n[3]=n3; n[4]=n4;
110  n[5]=n5; n[6]=n6; n[7]=n7; n[8]=n8; n[9]=n9;
111
112  dx = (1.0*W)/(1.0*nx);
113  C = dtau/(4.0*dx*dx);
114  wo = sqrt(zo);
115  printf("zo = %g\t tauw = %g\n", zo,tauw);
```

```
116
117  for(k=0;k<10;k++)
118   for(l=0;l<10;l++) {
119    Powerinitial[k][l]=0.0;
120    Powerfinal[k][l]=0.0;
121    cinitialr[k][l] = 0.0;
122    cinitiali[k][l] = 0.0;
123    c2maginitial[k][l] = 0.0;
124    cfinalr[k][l] = 0.0;
125    cfinali[k][l] = 0.0;
126    c2magfinal[k][l] = 0.0;
127    iS[k][l] = 0.0;
128    fS[k][l] = 0.0; }
129
130  for(x=0;x<nx;x++)
131   for(y=0;y<nx;y++) {
132    Atr[x][y] = 0.0;
133    Ati[x][y] = 0.0;
134    Atr_old[x][y] = 0.0;
135    Ati_old[x][y] = 0.0; }
136
137  for(k=0;k<10;k++)
138   for(l=0;l<10;l++)
139    for(i=0;i<nx;i++)
140     for(j=0;j<nx;j++){
141       Abinitialr[k][l][i][j] = 0.0;
142       Abinitiali[k][l][i][j] = 0.0;
143       Abfinalr[k][l][i][j] = 0.0;
144       Abfinali[k][l][i][j] = 0.0; }
145
146 /* Initializaitons complete ------------------*/
147 /* Loading basis set -------------------------*/
148
149  printf("\nLoading up basis sets at tau = 0.\n\n");
150
151  tau = 0.0;
152  wi = sqrt( zo + (tau-tauw)*(tau-tauw)/zo  );
153  printf("w(%g) = %g\n",tau,wi);
154
155  for(k=0;k<10;k++)
156   for(l=0;l<10;l++)
157    for(x=0;x<nx;x++)
```

```
158     for(y=0;y<nx;y++){
159       u = (sqrt(2)/wi)*(x - nx/2 + 0.5) * dx;
160       v = (sqrt(2)/wi)*(y - nx/2 + 0.5) * dx;
161       if (k==0) Hx=1.0;
162       if (k==1) Hx=2*u;
163       if (k==2) Hx=4*pow(u,2)-2;
164       if (k==3) Hx=8*pow(u,3)-12*u;
165       if (k==4) Hx=16*pow(u,4)-48*pow(u,2)+12;
166       if (k==5) Hx=32*pow(u,5)-160*pow(u,3)+120*u;
167       if (k==6) Hx=64*pow(u,6)-480*pow(u,4)+720*pow(u,2)-120;
168       if (k==7) Hx=128*pow(u,7)-1344*pow(u,5)+3360*pow(u,3)-1680*u;
169       if (k==8) Hx=256*pow(u,8)-3584*pow(u,6)+13440*pow(u,4)-13440*
170   pow(u,2)+1680;
171       if (k==9) Hx=512*pow(u,9)-9216*pow(u,7)+48384*pow(u,5)-80640*
172   pow(u,3)+30240*u;
173       if (l==0) Hy=1.0;
174       if (l==1) Hy=2*v;
175       if (l==2) Hy=4*pow(v,2)-2;
176       if (l==3) Hy=8*pow(v,3)-12*v;
177       if (l==4) Hy=16*pow(v,4)-48*pow(v,2)+12;
178       if (l==5) Hy=32*pow(v,5)-160*pow(v,3)+120*v;
179       if (l==6) Hy=64*pow(v,6)-480*pow(v,4)+720*pow(v,2)-120;
180       if (l==7) Hy=128*pow(v,7)-1344*pow(v,5)+3360*pow(v,3)-1680*v;
181       if (l==8) Hy=256*pow(v,8)-3584*pow(v,6)+13440*pow(v,4)-13440*
182   pow(v,2)+1680;
183       if (l==9) Hy=512*pow(v,9)-9216*pow(v,7)+48384*pow(v,5)-80640*
184   pow(v,3)+30240*v;
185
186       rsq = ((x-nx/2+0.5)*(x-nx/2+0.5)+(y-nx/2+0.5)*(y-nx/2+0.5))*dx*dx;
187       phi = (rsq*(tau-tauw)/(wo*wo*wi*wi)-(k+l+1)*atan((tau-tauw)/zo));
188
189       Abinitialr[k][l][x][y]=Ao*wo*Hx*Hy*exp(-rsq/(wi*wi))*cos(phi)/wi*
190       sqrt(1/(pow(2,k)*pow(2,l)*factorial(k)*factorial(l)));
191
192       Abinitiali[k][l][x][y]=Ao*wo*Hx*Hy*exp(-rsq/(wi*wi))*sin(phi)/wi*
193       sqrt(1/(pow(2,k)*pow(2,l)*factorial(k)*factorial(l)));
194
195       Powerinitial[k][l] = Powerinitial[k][l]+
196       Abinitialr[k][l][x][y]*Abinitialr[k][l][x][y] +
197       Abinitiali[k][l][x][y]*Abinitiali[k][l][x][y]; }
198
199 /* This serves as a check to ensure modes add up in the expected way */
```

```
200
201  printf("P_00(tau = 0) = %g\n",Powerinitial[0][0]);
202
203
204
205 /* forming initial At @ tau = 0 ---------------------------------*/
206  for(i=0;i<10;i++)
207   for(x=0;x<nx;x++)
208    for(y=0;y<nx;y++) {
209     Atr[x][y] = Atr[x][y] + c[i]*Abinitialr[m[i]][n[i]][x][y];
210     Ati[x][y] = Ati[x][y] + c[i]*Abinitiali[m[i]][n[i]][x][y]; }
211
212 /* finding total power in At */
213
214  for(x=0;x<nx;x++)
215   for(y=0;y<nx;y++)
216    P0 = P0 + Atr[x][y]*Atr[x][y] + Ati[x][y]*Ati[x][y];
217
218  printf("P_T(0) = %g\n",P0);
219  printf("Outputting initial wavefront to file\n\n");
220
221 /* Output At cross section to file and saving old values*/
222
223  for(x=0;x<nx;x++) {
224   for(y=0;y<nx;y++) {
225    ampinitial = sqrt( Atr[x][y]*Atr[x][y] + Ati[x][y]*Ati[x][y] );
226    Atr_old[x][y] = Atr[x][y];
227    Ati_old[x][y] = Ati[x][y];
228    fprintf(initial, "%lf ",ampinitial);  }
229   fprintf(initial, "\n");  }
230
231 /* Cmn calculation for initial waveform----------------------*/
232
233  printf("Calculating initial Cmns\n");
234
235  K = (2*dx*dx)/(pi*zo);
236  for(k=0;k<10;k++)
237   for(l=0;l<10;l++)
238    for(x=0;x<nx;x++)
239     for(y=0;y<nx;y++) {
240      cinitialr[k][l] = cinitialr[k][l] + K *
241        (Atr[x][y]*Abinitialr[k][l][x][y] +
```

```
242     Ati[x][y]*Abinitiali[k][l][x][y]);
243
244      cinitiali[k][l] = cinitiali[k][l] + K *
245        (Ati[x][y]*Abinitialr[k][l][x][y] -
246     Atr[x][y]*Abinitiali[k][l][x][y]);}
247
248
249 /* calculating Cmn squared */
250  for(k=0;k<10;k++)
251   for(l=0;l<10;l++) {
252    c2maginitial[k][l] = (cinitialr[k][l]*cinitialr[k][l]+
253    cinitiali[k][l]*cinitiali[k][l]);
254    c2sumInitial = c2sumInitial +  c2maginitial[k][l]; }
255
256  printf("\nNormalized initial cmn amplitudes squared\n");
257
258  for(k=0;k<10;k++)
259   for(l=0;l<10;l++) {
260    iS[k][l] = c2maginitial[k][l]/c2sumInitial;
261    if (iS[k][l] > 0.01) printf("Cmn2[%d][%d] = %g\n",k,l,iS[k][l]); }
262
263
264 /* propagation of At from tau = 0 to tau= 1 */
265
266  printf("\nPropagating waveform...\n\n");
267
268  for(tau=0.0;tau<=0.9999;tau=tau+dtau) {/* start tau loop */
269
270 /* wave equation over x,y and tau */
271   for(y=1;y<nx-1;y++)
272    for(x=1;x<nx-1;x++){
273    Atr[x][y] = Atr[x][y]-C*(Ati_old[x+1][y]+Ati_old[x-1][y]+
274    Ati_old[x][y+1]+Ati_old[x][y-1]-4.0*Ati_old[x][y]);
275
276    Ati[x][y] = Ati[x][y]+C*(Atr_old[x+1][y]+Atr_old[x-1][y]+
277    Atr_old[x][y+1]+Atr_old[x][y-1]-4.0*Atr_old[x][y]); }
278
279    /* saving old values */
280    for(x=0;x<nx;x++)
281     for(y=0;y<nx;y++){
282      Atr_old[x][y] = Atr[x][y];
283      Ati_old[x][y] = Ati[x][y]; }
```

```
284
285 /* y vs. tau output */
286    if (count1==100) {
287     count1=0;
288    for(y=0;y<nx;y++) {
289     ampy = sqrt (Atr[nx/2][y]*Atr[nx/2][y] + Ati[nx/2][y]*Ati[nx/2][y]);
290     fprintf(ytau,"%g ",ampy); } }
291
292   fprintf(ytau,"\n");
293
294   count1 = count1 + 1;  } /*end tau loop */
295
296 /* output for final waveform */
297  for(x=0;x<nx;x++) {
298   for(y=0;y<nx;y++){
299    ampfinal = sqrt( Atr[x][y]*Atr[x][y] + Ati[x][y]*Ati[x][y] );
300    fprintf(final,"%g ",ampfinal); }
301
302   fprintf(final,"\n"); }
303
304
305 /* Calculating cmns for final waveform (i.e., after propagation)----- */
306 /* Must create basis set at tau = 1.0 */
307
308  wf = sqrt( zo + (tau-tauw)*(tau-tauw)/zo  );
309  printf("w(%g) = %g\n",tau,wf);
310
311
312  for(k=0;k<10;k++)
313   for(l=0;l<10;l++)
314    for(x=0;x<nx;x++)
315     for(y=0;y<nx;y++){
316      u = (sqrt(2)/wf)*(x - nx/2 + 0.5) * dx;
317      v = (sqrt(2)/wf)*(y - nx/2 + 0.5) * dx;
318  if (k==0) Hx=1.0;
319  if (k==1) Hx=2*u;
320  if (k==2) Hx=4*pow(u,2)-2;
321  if (k==3) Hx=8*pow(u,3)-12*u;
322      if (k==4) Hx=16*pow(u,4)-48*pow(u,2)+12;
323      if (k==5) Hx=32*pow(u,5)-160*pow(u,3)+120*u;
324      if (k==6) Hx=64*pow(u,6)-480*pow(u,4)+720*pow(u,2)-120;
325      if (k==7) Hx=128*pow(u,7)-1344*pow(u,5)+3360*pow(u,3)-1680*u;
```

```
326      if (k==8) Hx=256*pow(u,8)-3584*pow(u,6)+13440*pow(u,4)-13440*
327  pow(u,2)+1680;
328      if (k==9) Hx=512*pow(u,9)-9216*pow(u,7)+48384*pow(u,5)-80640*
329  pow(u,3)+30240*u;
330      if (l==0) Hy=1.0;
331      if (l==1) Hy=2*v;
332      if (l==2) Hy=4*pow(v,2)-2;
333      if (l==3) Hy=8*pow(v,3)-12*v;
334  if (l==4) Hy=16*pow(v,4)-48*pow(v,2)+12;
335      if (l==5) Hy=32*pow(v,5)-160*pow(v,3)+120*v;
336      if (l==6) Hy=64*pow(v,6)-480*pow(v,4)+720*pow(v,2)-120;
337      if (l==7) Hy=128*pow(v,7)-1344*pow(v,5)+3360*pow(v,3)-1680*v;
338      if (l==8) Hy=256*pow(v,8)-3584*pow(v,6)+13440*pow(v,4)-13440*
339  pow(v,2)+1680;
340      if (l==9) Hy=512*pow(v,9)-9216*pow(v,7)+48384*pow(v,5)-80640*
341  pow(v,3)+30240*v;
342
343      rsq = ((x-nx/2+0.5)*(x-nx/2+0.5)+(y-nx/2+0.5)*(y-nx/2+0.5))*dx*dx;
344      phi = ( rsq*(tau-tauw)/(wo*wo*wf*wf)-(k+l+1)*atan((tau-tauw)/zo) );
345
346      Abfinalr[k][l][x][y] = Ao * wo * Hx * Hy * exp(-rsq/(wf*wf)) *
347      cos(phi)/wf*sqrt(1/(pow(2,k)*pow(2,l)*factorial(k)*factorial(l)));
348
349      Abfinali[k][l][x][y] = Ao * wo * Hx * Hy * exp(-rsq/(wf*wf)) *
350      sin(phi)/wf*sqrt(1/(pow(2,k)*pow(2,l)*factorial(k)*factorial(l)));
351
352  Powerfinal[k][l] = Powerfinal[k][l] +
353  Abfinalr[k][l][x][y]*Abfinalr[k][l][x][y] +
354  Abfinali[k][l][x][y]*Abfinali[k][l][x][y]; }
355
356  printf("P_00(1) = %g\n",Powerfinal[0][0]);
357
358 /* Finding total power in At at tau=1 *(should equal the tau=0 case)*/
359  for(x=0;x<nx;x++)
360   for(y=0;y<nx;y++)
361    P1 = P1 + Atr[x][y]*Atr[x][y] + Ati[x][y]*Ati[x][y];
362
363  printf("P_T(1) = %g\n", P1);
364
365 /* orthogonality calculation */
366  K = (2*dx*dx)/(pi*zo);
367  for(k=0;k<10;k++)
```

```
368   for(l=0;l<10;l++)
369    for(x=0;x<nx;x++)
370     for(y=0;y<nx;y++) {
371      cfinalr[k][l] = cfinalr[k][l] + K *
372      (Atr[x][y]*Abfinalr[k][l][x][y] + Ati[x][y]*Abfinali[k][l][x][y]);
373
374      cfinali[k][l] = cfinali[k][l] + K *
375      (Ati[x][y]*Abfinalr[k][l][x][y] - Atr[x][y]*Abfinali[k][l][x][y]);}
376
377 /* calculating cmn squared */
378  for(k=0;k<10;k++)
379   for(l=0;l<10;l++) {
380    c2magfinal[k][l] = (cfinalr[k][l]*cfinalr[k][l] +
381                        cfinali[k][l]*cfinali[k][l]);
382    c2sumFinal = c2sumFinal +  c2magfinal[k][l];}
383
384  printf("\nNormalized initial cmn amplitudes squared\n");
385  for(k=0;k<10;k++)
386   for(l=0;l<10;l++) {
387    fS[k][l] = c2magfinal[k][l]/c2sumFinal;
388    if (fS[k][l] > 0.01) printf("Cmn2[%d][%d] = %g\n",k,l,fS[k][l]);}
389  printf("\n");
390  printf("\nClosing files...\n");
391  fclose(input);
392  fclose(initial);
393  fclose(final);
394  fclose(ytau);
395
396 } /*end main() */
397
398 int factorial(int a)
399  {
400   if ((a==1) || (a==0))
401    return 1;
402   else {
403    a *= factorial(a-1);
404    return a; } }
405 /* End of Cmn.c */
```

2. CMN.IN – INPUT FILE

```
/* Begin input file */
     1 1 0 2
     2 1 2 0
     3 0 0 2
     4 0 4 0
     5 0 0 4
     6 0 2 7
     7 0 4 9
     8 0 3 8
     9 0 5 3
    10 0 0 6
    11 1.0 10 100
    12 0.5 1.0 400E-6
    13 %c0 m0 n0
    14 %c1 m1 n1
    15 %c2 m2 n2
    16 %c3 m3 n3
    17 %c4 m4 n4
    18 %c5 m5 n5
    19 %c6 m6 n6
    20 %c7 m7 n7
    21 %c8 m8 n8
    22 %c9 m9 n9
    23 %Ao W nx
    24 %zo tauw dtau
/* End input file */
```

3. COEFFS.M – MATLAB SCRIPT

```
     1 close all
     2 clear
     3 clc
     4 load initial.out
     5 load final.out
     6 load Cmn.in
     7 load ytau.out;
     8
     9
    10 ytau = ytau';
    11 initial = initial';
    12 final = final';
```

```
13
14
15 W = Cmn(11,2);
16 nx = Cmn(11,3);
17 dtau = Cmn(12,3);
18 tau=0:dtau:1-dtau;
19 x = 0:1:nx-1;
20
21 [npx,timesteps] = size(ytau);
22 dtau = 1/timesteps;
23 tau = 0:dtau:1-dtau;
24 x = 0:1:npx-1;
25
26
27 [x_initial,y_initial]=meshgrid(0:W/nx:W-W/nx);
28 [x_final,y_final]=meshgrid(0:W/nx:W-W/nx);
29
30
31 figure('Color','white')
32 set(gca,'FontSize',25)
33 pcolor(x_initial,y_initial,initial)
34 colorbar
35 axis square
36 shading flat
37 shading interp
38 title('initial waveform')
39 xlabel('x')
40 ylabel('y')
41 colormap(hot)
42
43 figure('Color','white')
44 set(gca,'FontSize',25)
45 surf(initial)
46 title('initial surface plot')
47 xlabel('x')
48 ylabel('y')
49 zlabel('a_i*a_i')
50 colormap(hot)
51
52 figure('Color','white')
53 set(gca,'FontSize',25)
54 pcolor(x_final,y_final,final)
```

```
55 xlabel('x')
56 ylabel('y')
57 colorbar
58 axis square
59 shading flat
60 shading interp
61 title('final waveform')
62 colormap(hot)
63
64 figure('Color','white')
65 set(gca,'FontSize',25)
66 surf(final)
67 xlabel('x')
68 ylabel('y')
69 zlabel('a_f*a_f*')
70 title('final surface plot')
71 colormap(hot)
72
73 figure('Color','white')
74 set(gca,'FontSize',25)
75 [Tau,X]=meshgrid(tau,x);
76 pcolor(Tau,X,ytau)
77 shading flat
78 shading interp
79 title('Laser amplitude y  vs.  \tau')
80 xlabel('\tau')
81 ylabel('x')
82 colormap(hot)
```

THIS PAGE INTENTIONALLY LEFT BLANK

APPENDIX B. USEFUL RELATIONS

Quick reference for some important equations

1. FREE ELECTRON LASER OVERVIEW

Resonance Condition	$\lambda = \lambda_o \frac{(K^2+1)}{2\gamma^2}$	Equation (II.1)
Gain	$G = \frac{P-P_o}{P_o}$	Equation (II.2)
Extraction	$\eta = \frac{\text{Optical power}}{\text{Initial electron beam power}}$	Equation (II.3)

2. FREE ELECTRON LASER THEORY

Pendulum Equation	$\overset{\circ\circ}{\zeta} = \lvert a \rvert \cos(\zeta + \phi)$	Equation (III.32)
Power	$P = \lvert a \rvert^2$	Equation (III.37)
FEL wave equation	$\left[-\frac{i}{4}\tilde{\boldsymbol{\nabla}}^{\mathbf{2}}_{\perp} + \frac{\partial}{\partial\tau}\right] a(\tilde{\mathbf{r}},\tau) = < -je^{-i\zeta} >$	Equation (III.64)

3. OPTICAL THEORY

F. Trial Solution	$a = a_o e^{-\left(p+\frac{\tilde{r}^2}{\tilde{z}_o q}\right)}$	Equation (IV.3)
F. Solution	$a = a_o \frac{w_o}{w} e^{-\frac{\tilde{r}^2}{w^2}} e^{i\left(\frac{\tilde{r}^2 \tau}{w_o^2 w^2} - \arctan\frac{\tau}{\tilde{z}_o}\right)}$	Equation (IV.20)
HOM Trial Solution	$a = a_o g h e^{-(p+\frac{\tilde{r}^2}{\tilde{z}_o q})}$	Equation (IV.24)
HG Mode Solution	$a_{m,n} = a_o \frac{w_o}{w} H_m H_n e^{-\frac{\tilde{r}^2}{w^2}} e^{i\phi_{m,n}}$	Equation (IV.45)
HOM Phase	$\phi_{m,n} = \frac{\tilde{r}^2 \tau}{w_o^2 w^2} - (m+n+1)\arctan\frac{\tau}{\tilde{z}_o}$	Equation(IV.46)
Normalized HG mode	$A_{m,n} = \frac{1}{\sqrt{2^m 2^n m! n!}} a_{m,n}$	Equation (IV.60)
Total field HG	$A_T = \sum_{m,n}^{\infty} C_{m,n} A_{m,n}$	Equation (IV.61)
Normalized Coefficients	$C_{m,n} = \frac{2}{\pi a_o^2 w_o^2} \int_{-\infty}^{\infty} \int_{-\infty}^{\infty} A_T \, A_{m,n}^{*} \, d\tilde{x} d\tilde{y}$	Equation (IV.66)

4. SIMULATIONS

Total Power in optical field	$P_T = \frac{\pi}{2} a_o^2 w_o^2 \sum_{m,n}^{\infty} C_{m,n}^2$	Equation (V.13)
Fractional Power Spectrum	$S[m][n] = \frac{C[m][n]^2}{\sum_{i,j} C[i][j]}$	Equation (V.15)

LIST OF REFERENCES

[1] Thomas Jefferson Lab National Facility. Free electron laser systems diagram. *http://www.jlab.org/FEL/feldescrip.html*, 12 April 2006.

[2] C. A. Brau. *Free-Electron Lasers.* Academic Press, INC., 1990.

[3] Thomas Jefferson Lab National Facility. Jlab operating parameters. *Directed Energy Professional Society Proceedings*, November 2005.

[4] N. Thompson. Introduction to free-electron lasers. Technical report, Accelerator Science and Technology Centre, 2003.

[5] B. Williams. Higher-order modes in free electron lasers. Master's thesis, Naval Postgraduate School, 2005.

[6] P. O'Shea. Introduction to free-electron lasers. *Directed Energy Professional Society Short Course*, 2003.

[7] Thomas Jefferson Lab National Facility. Free electron laser linear accelerator. *http://education.jlab.org/sitetour/fellinac.html*, 12 April 2006.

[8] Hahn-Meitner Institute (HMI). Undulator designs. *http://www.hmi.de/bereiche/SF/SF2/arbeitsg/bessy/sf204ab.html*, 13 April 2006.

[9] National Laboratory for High Energy Physics (KEK). Free electron laser beam dump. *http://www-ps.kek.jp/jhf-np/hadronbeam/dump/beamdump.jpg*, 13 April 2006.

[10] J. D. Jackson. *Classical Electrodynamics.* John Wiley and Sons, Inc., third edition edition, 1999.

[11] C. A. Brau. *Modern Problems In Classical Electrodynamics.* Oxford University Press, 2004.

[12] M. Abramowitz and I. A. Stegun, editors. *Handbook of Mathematical Functions.* Dover, 1972.

[13] W. B. Colson. *Free Electron Laser Theory.* PhD thesis, Stanford University, 1977.

[14] D. J. Griffiths. *Introduction to Electrodynamics.* Prentice Hall, 1999.

[15] L. D. Landau and Lifschitz. *Fluid Mechanics.* Oxford, England: Pergamon Press, 1982.

[16] H. Kogelnik and T. Li. Laser beams and resonantors. *Applied Optics*, 5(10), 1966.

[17] R. H. Hardin and F. D. Tappert. Applications of the split-step fourier method to the numerical solution of nonlinear and variable coefficient wave equation. *SIAM Rev*, 15(423), 1973.

[18] C. Pellegrini W. B. Colson and A. Renieri, editors. *Free Electron Laser Handbook*. North-Holland Physics, 1990.

[19] W. Silfvast. *Laser Fundamentals*. Cambridge University Press, second edition edition, 2004.

INITIAL DISTRIBUTION LIST

1. Defense Technical Information Center
   Ft. Belvoir, VA

2. Dudley Knox Library
   Naval Postgraduate School
   Monterey, CA

3. CAPT David Kiel
   Naval Sea Systems Command PMS-405
   Washington, DC

4. CAPT (ret) Roger McGinnis
   Office of Naval Research
   Arlington, VA

5. Dr. Starnes Walker
   Office of Naval Research
   Arlington, VA

6. Quentin Saulter
   Office of Naval Research
   Arlington, VA

7. Dr. Alan Todd
   Advanced Energy Systems, Inc.
   Princeton, NJ

8. Dr. Fred Dylla
   Thomas Jefferson National Accelerator Facility
   Newport News, VA

9. Dr. George Neil
   Thomas Jefferson National Accelerator Facility
   Newport News, VA

10. Chairman, Physics Department
    Naval Postgraduate School
    Monterey, CA

11. Professor William Colson
    Naval Postgraduate School
    Monterey, CA

12. Professor Robert Armstead
    Naval Postgraduate School
    Monterey, CA

13. Professor Joseph Blau
    Naval Postgraduate School
    Monterey, CA

14. Professor Peter Crooker
    Naval Postgraduate School
    Monterey, CA

15. Professor Wayne Roberge
    Rensselaer Polytechnic Institute
    Troy, Ny

16. Professor Dan Gefroh
    Hawaii Pacific University
    Honolulu, Hawai'i